QUARTERLY OF APPLIED MATHEMATICS
https://doi.org/10.1090/qam/1567
Article electronically published on January 22, 2020

ACTIVE MANIPULATION OF EXTERIOR ELECTROMAGNETIC FIELDS BY USING SURFACE SOURCES

By

DANIEL ONOFREI (*Department of Mathematics, University of Houston, Houston, Texas 77004*),

ERIC PLATT (*Department of Mathematics, University of Houston, Houston, Texas 77004*),

AND

NEIL JEROME A. EGARGUIN (*Institute of Mathematical Sciences and Physics, University of the Philippines Los Baños, College, Laguna, Philippines; and Department of Mathematics, University of Houston, Houston, Texas 77004*)

Abstract. In this paper, we establish a scheme for the active manipulation of electromagnetic fields in prescribed exterior regions using a surface source. We prove the existence of the necessary surface current (electric or magnetic) on a single source to approximate prescribed electromagnetic fields on given regions of space (bounded or possibly the far field). We provide two constructive schemes for the computation of the required surface currents: our first strategy makes use of the Debye representation results for the electromagnetic field and builds up on previous control results for scalar fields discussed in [J. Integral Equations Appl. 26 (2014), pp. 553–579]; the second strategy we propose makes use of integral electromagnetic representation results and follows theoretically from the first. We provide theoretical validation for both computational schemes and present supporting numerical simulations for the first strategy in several applied scenarios.

1. Introduction. The study of electromagnetic waves has been a very popular subject of research due to its far-reaching applications, from remote sensing, biomedical engineering and imaging to radar systems, defense, and warfare. A good amount of research in this area deals with the design and implementation of accurate and efficient numerical methods to solve electromagnetic problems such as those in the analysis of

Received October 22, 2019, and, in revised form, November 25, 2019.
2010 *Mathematics Subject Classification.* Primary 35Q60, 45Q05.
Key words and phrases. Control of EM waves, Maxwell's equations, Debye potentials, integral equations in inverse problems, near and far field synthesis, Tikhonov regularization.
The authors would like to acknowledge the Army Research Office for funding this work under the award W911NF- 17-1-0478.
Email address: onofrei@math.uh.edu
Email address: eplatt314@gmail.com
Email address: naegarguin1@up.edu.ph

large scale systems [29], [26], [39], scattering analysis [66], [2], [62], [63], [68], and inverse problems (see for instance [18], [64], [19]).

Theoretically, the controllability of Maxwell's equations within dielectric bodies through control of surface currents was studied in [35], [48] and [18]. These authors have used the Hilbert Uniqueness Method of Lions [38] concerning the control of systems and partial differential equations. Recent works on the interior control problem in various geometric configurations and/or specific media using surface currents include [33], [34], [57], [15], [8]. The reference books [10] and [36] offer a comprehensive description of important results on feedback control laws for general hyperbolic infinite dimensional systems through the use of abstract Riccati equations.

Our work on active control strategies for exterior electromagnetic fields are motivated by practical applications, such as scattering cancellation or field synthesis.

In scattering cancellation applications, it is assumed that a given target is interrogated by an incident field and requires the construction of necessary boundary currents for the partial or total cancellation of the resulting scattered field. Some works concerning this application include [50] where a detailed sensitivity analysis is presented and [59, 60] where the electromagnetic equivalence principle is used to show how a dipole array can cancel the known scattered field from a cylinder. The authors in [42], [41], and [43] studied the structure of non-radiating sources while those of [3], [21], and [20] considered their applications for active cloaking. Experimental results on active cloaking are presented in [40] for quasistatic regime and in [24] for finite frequency regime. In a recent review paper [28], the authors describe a strategy which make use of electromagnetic equivalence principles to show how electromagnetic fields can be actively manipulated in given regions of free space by using surface distributed active elements (obtaining an alternative characterization of the so-called Huygens' Metasurfaces).

The other class of applications is on field synthesis. Classically, the problem of field synthesis requires the construction of necessary currents on an active source for the approximation of a given far field pattern [7] ("the far field synthesis"). In our formulation below, the field synthesis problem requires the construction of necessary currents on the source for the approximation of various prescribed solutions of Maxwell equations in various given exterior regions (possibly including, but not limited to, the far field region). The problem of far field synthesis is well studied in the mathematical literature. For instance, the monograph [7] presents a detailed discussion of optimization procedures for the various related questions. The near field synthesis problem, on the other hand, is mostly discussed in the engineering literature and in the review [12], the authors summarized the recent progress on this problem and proposed a genetic optimization algorithm based on the far field to near field mapping for a solution. The monograph [31] discusses the use of far field to near field mapping in near field scanning applications.

Another approach to the control problem in the context of the above-mentioned applications is the use of novel composites for various control strategies based on transformation acoustics and transformation optics techniques. In this regard, starting with the works [30], [54], [17] (see also [23] where the idea of transformation invariance of Maxwell equations was first used to compare EM fields in different structures), in recent years there had been many research insights in the field of acoustic and electromagnetic

metamaterials. For example, the monographs [58], [11], [27], [55], [16] and the references therein offer insightful perspectives on the history, foundations, recent advances, and possible applications of metamaterials. The effects of small heterogeneities and other peculiar properties of metamaterials to proposed control strategies had also been studied in [5], [4], [6] and the references therein.

This paper proposes a new approach in the active control of electromagnetic fields to characterize the necessary surface currents on a single source to produce the desired fields on prescribed exterior regions of space. Two possible computation schemes are discussed: the first scheme is based on expressing the desired (vector) fields in terms of (scalar) Debye potentials; the second strategy is based on using integral representation results for the electromagnetic fields to reduce the problem to solving a series of integral equations for certain electromagnetic moments. While we theoretically validate both solution approaches we focus numerically only on the first approach offering supportive simulations in several applied scenarios.

More explicitly, the first approach proposed in the paper gives rise to a pair of scalar inverse source problems involving the Helmholtz equation as discussed in [52], [53], and [25]. The solutions obtained for these inverse problems are then used to find the boundary currents that will radiate an approximation of the prescribed electric and magnetic fields on the given exterior regions. Regarding this approach we mention that the use of the Debye decomposition for the electromagnetic field is not a new idea (see [37, 44–47, 49, 51, 56, 61, 67]). In fact, in [61] the author observed that in order to characterize electromagnetic diffraction phenomena around a conical boundary it is enough to solve the associated scalar problems for the two corresponding Debye potentials. But, to the best of our knowledge, the use of Debye decomposition in corroboration with smooth control results of the Helmholtz equation for a unified strategy for the active manipulation of electromagnetic fields is a novel alternative approach which we believe presents several important appealing qualities: constructiveness (which makes it computationally friendly); simplicity, since it relies heavily only on the analysis for the scalar case; generality, since it provides a unifying platform for many interesting applications; feasibility, since by design it offers the possibility to successfully understand possible discrete approximation methods for instantiation of the continuous surface currents theoretically predicted.

The rest of the paper is organized as follows: Section 2 formally presents the problem and states the paper's main result, Theorem 2.1. Section 3 presents the proof of the main result by two alternative approaches and highlights some important consequences of the results. Section 4 establishes a framework for the numerical implementation of the theoretical results based on the first solution approach presented in Section 3. This includes the description of the spherical harmonic decomposition of the prescribed electric and magnetic fields and some analytic calculations that will make the numerical simulation more accurate. This numerical framework is implemented and the results are presented in Section 5. Finally, in Section 6, we offer some concluding remarks and some possible future research directions.

2. Main result. In this section we introduce the geometry and functional framework of our problem and state our main result. In this regard, denote by $D_s \Subset \mathbb{R}^3$ the open and connected source domain with a Liptschitz boundary, modeled as a surface current on ∂D_s. In order to streamline the presentation, in what follows we will assume that the media surrounding D_s is air and denote by B_r the ball centered at the origin and radius r (but any homogeneous and isotropic surrounding media will fit within the framework of our presentation). Consider $M \in \mathbb{N}$ smooth mutually disjoint control domains $\{D_1, \dots, D_M\}$ in $\mathbb{R}^3$ and let D_0 be a domain including the origin such that $\bigcup_i D_i \cup \overline{D}_s \Subset B_R \Subset D_0$ for some large enough R (where here and in the rest of the document $\Subset$ denotes compact inclusion). In what follows, $\{D_1, \dots, D_M\}$ and $\mathbb{R}^3 \setminus D_0$ will be referred to as the control regions. Note that in the case of scattering cancellation application, $D_i = \emptyset$ for each $i \geq 1$. Next, we make the assumption that D_s and the regions of control D_i are well separated,

$$\overline{D}_i \cap \overline{D}_s = \emptyset \text{ for each } i = \overline{1, M}. \tag{2.1}$$

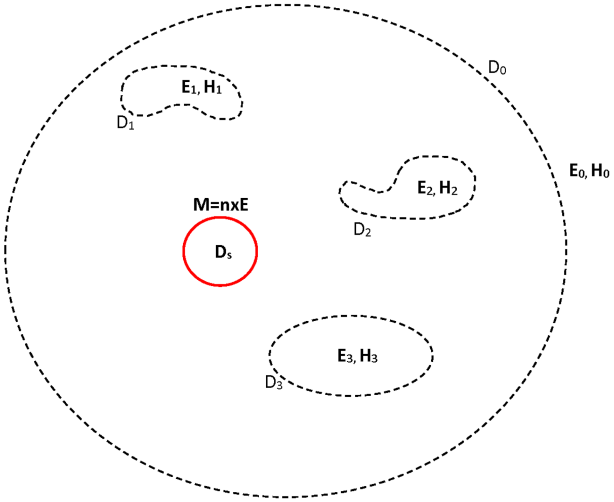

FIG. 1. Diagram of electromagnetic active field manipulation.

A sketch of the problem geometry is presented in Figure 1 where only four domains $\{D_0, D_1, D_2, D_3\}$ are represented and the source D_s is modeled as a surface magnetic current. We consider wave propagation in a homogeneous isotropic source free non-conductive medium in $\mathbb{R}^3$. The time-domain Maxwell system reads ([9]):

$$\nabla \times \mathbf{E} = -\mu \frac{\partial \mathbf{H}}{\partial t}; \nabla \times \mathbf{H} = \varepsilon \frac{\partial \mathbf{E}}{\partial t}, \tag{2.2}$$

where μ, ε are the magnetic permeability and electric permitivity of the homogeneous and isotropic ambient space. In the time-harmonic case considered in this paper, the e^{-iwt} time dependence is assumed but suppressed in what follows and thus the system (2.2) becomes

$$\nabla \times \mathbf{E} = i\mu\omega \mathbf{H}; \nabla \times \mathbf{H} = -i\omega\varepsilon \mathbf{E}. \tag{2.3}$$

Let B_R as above and consider $M+1$ pairs of vector functions $\{(\mathbf{E}_i, \mathbf{H}_i)\}_{i=0}^{n}$ such that:

$$\begin{aligned} &(\mathbf{E}_i, \mathbf{H}_i) \quad \text{solve Maxwell system in annular source free regions } \Sigma_i \text{ centered in the origin and with } D_i \Subset \Sigma_i \text{ for } 1 \le i \le M, \\ &(\mathbf{E}_0, \mathbf{H}_0) \text{ is a radiating solution of the Maxwell system in } \Sigma_0 = \mathbb{R}^3 \setminus B_R, \end{aligned} \tag{2.4}$$

where by a radiating solution of Maxwell equations we understand a solution which satisfies the Silver-Muller radiation conditions at infinity, i.e.,

$$\begin{aligned} \mathbf{E}(\mathbf{x}) \times \hat{\mathbf{x}} + \frac{1}{Y}\mathbf{H}(\mathbf{x}) &= O(1/|\mathbf{x}|^2), \\ \mathbf{H}(\mathbf{x}) \times \hat{\mathbf{x}} - Y\mathbf{E}(\mathbf{x}) &= O(1/|\mathbf{x}|^2), \end{aligned} \tag{2.5}$$

as $|\mathbf{x}| \to \infty$ uniformly with respect to $\hat{\mathbf{x}} \in S^2$ and where $Y = \sqrt{\frac{\varepsilon}{\mu}}$ denotes the admittance in non-conductive media (see [9], [7]). The radiation conditions can be simply rewritten for all the equivalent forms of the Maxwell system (see Section 3) and giving a smooth enough boundary data, they guarantee uniqueness of solutions for Maxwell exterior problems [13].

The main result of the paper regards the theoretical possibility to characterize needed input data on the boundary of the active source domain D_s (i.e., conduction or magnetic surface currents) so that given desired fields are well approximated in prescribed bounded or unbounded mutually disjoint exterior regions of space. We have the following.

THEOREM 2.1. Let $0 < \delta \ll 1$ be fixed and consider domains D_s and $\{D_i\}_{i=0}^{M}$ as above. Also, let $(\mathbf{E}_0, \mathbf{H}_0)$ and $(\mathbf{E}_i, \mathbf{H}_i)$ with $1 \le i \le M$ as in (2.4). Then there exists smooth surface magnetic currents $\mathbf{M} \in C^\infty(\partial D_s)$ (or smooth conduction currents $\mathbf{J} \in C^\infty(\partial D_s)$) such that the solutions $(\mathbf{E}, \mathbf{H})$ of

$$\begin{cases} \nabla \times \mathbf{E} = i\mu\omega\mathbf{H};\ \nabla \times \mathbf{H} = -i\omega\varepsilon\mathbf{E} & \text{in } \mathbb{R}^3 \setminus \bar{D}_s, \\ \mathbf{E} \times \mathbf{n} = \mathbf{M} \text{ (or } \mathbf{H} \times \mathbf{n} = \mathbf{J}) & \text{on } \partial D_s, \\ (\mathbf{E}, \mathbf{H}) \text{ satisfy the Silver-Muller radiation condition at infinity,} \end{cases} \tag{2.6}$$

where $\mathbf{n}$ is the unit exterior normal to D_s, satisfy

$$\begin{aligned} &\|\mathbf{E} - \mathbf{E}_0\|_{C(\mathbb{R}^3 \setminus D_0)} \le C\delta, \quad \|\mathbf{E} - \mathbf{E}_i\|_{C(\overline{D_i})} \le C\delta \text{ for each } i = \overline{1, M}, \\ &\|\mathbf{H} - \mathbf{H}_0\|_{C(\mathbb{R}^3 \setminus D_0)} \le C\delta, \quad \|\mathbf{H} - \mathbf{H}_i\|_{C(\overline{D_i})} \le C\delta \text{ for each } i = \overline{1, M}, \end{aligned} \tag{2.7}$$

where the constant C above depends only on ω, ε, μ.

3. Proof of the theorem and some further discussions. In this section we present the proof of Theorem 2.1 in the case of a source domain D_s modeled by a magnetic surface current $\mathbf{M} = \mathbf{E} \times \mathbf{n}$ on ∂D_s mentioning that the case of a source modeled by a conduction current $\mathbf{J} = \mathbf{H} \times \mathbf{n}$ follows similarly. We then present two approaches for the numerical computation of the required surface currents with the note that the second computation strategy will give us the opportunity to include a discussion about the possibility that the source allows for both types of surface currents, conduction and magnetic.

Proof. Our arguments for the proof of Theorem 2.1 make use of previous scalar control results obtained in [52], [53],[25], [32] together with representation results of the electromagnetic field.

In what follows we will make use of two other forms of the Maxwell system. In this regard, from (2.3) it can be easily observed that $\tilde{\mathbf{E}} = \sqrt{\epsilon}\ \mathbf{E}, \tilde{\mathbf{H}} = \sqrt{\mu}\ \mathbf{H}$ equivalently satisfy

$$\nabla \times \tilde{\mathbf{E}} = ik\tilde{\mathbf{H}}; \nabla \times \tilde{\mathbf{H}} = -ik\tilde{\mathbf{E}} \tag{3.1}$$

and that $\mathbf{A} = \sqrt{-i\epsilon\omega}\ \mathbf{E}, \mathbf{B} = \sqrt{i\omega\mu}\ \mathbf{H}$ equivalently satisfy

$$\nabla \times \mathbf{A} = k\mathbf{B}; \nabla \times \mathbf{B} = k\mathbf{A}, \tag{3.2}$$

where here the principal branch of the logarithm was used in the definition of the complex square root above and in the last two equations, $k = \omega\sqrt{\varepsilon\mu}$ denotes the associated wave number. In light of (3.2), it was shown in [65] that there exists unique u_i, v_i (with zero average over the unit ball) solutions of the Helmholtz equation in Σ_i for each $i \in \{0, \dots, M\}$ given by the following weakly singular integral operators:

$$\begin{aligned} u_i(r\hat{\mathbf{r}}) &= -\frac{r}{2\pi}\int_{B_1}\Big(\log(\sin\frac{\gamma}{2})\Big)\,\hat{\mathbf{r}}\cdot\mathbf{A}_i(r\hat{\mathbf{r}'})d\sigma', \\ v_i(r\hat{\mathbf{r}}) &= -\frac{r}{2\pi}\int_{B_1}\Big(\log(\sin\frac{\gamma}{2})\Big)\,\hat{\mathbf{r}}\cdot\mathbf{B}_i(r\hat{\mathbf{r}'})d\sigma', \end{aligned} \tag{3.3}$$

where $\mathbf{A}_i = \sqrt{-i\epsilon\omega}\ \mathbf{E}_i, \mathbf{B}_i = \sqrt{i\omega\mu}\ \mathbf{H}_i$, $\hat{\mathbf{r}}$ denotes the unit vector along direction $\mathbf{r}$, $r = |\mathbf{r}|$, γ denotes the geodesic distance between $\hat{\mathbf{r}}$ and $\hat{\mathbf{r}}'$, and $u_i(\mathbf{r}), v_i(\mathbf{r})$ satisfy

$$\mathbf{A}_i(\mathbf{r}) = \nabla\times(\nabla\times u_i\mathbf{r}) + k\nabla\times v_i\mathbf{r},\ \ \mathbf{B}_i(\mathbf{r}) = \nabla\times(\nabla\times v_i\mathbf{r}) + k\nabla\times u_i\mathbf{r}\ \text{ in } \Sigma_i \tag{3.4}$$

for each $i \in \{0, \dots, M\}$ where the sets Σ_i for $i \in \{0, \dots, M\}$ were introduced in (2.4). Moreover, it was shown in [65] that the radiation condition satisfied by $(\mathbf{E}_0, \mathbf{H}_0)$ implies that (u_0, v_0) is a radiating solution of the Helmholtz equation in $\Sigma_0 = \mathbb{R}^3 \setminus B_R$. Next we make the observation that the results in [52] (see also [32], [53], [25]) can be immediately adapted to obtain the following smooth control result.

THEOREM 3.1. Let $0 < \delta \ll 1$ be fixed and consider the Debye potentials u_i, v_i for $i \in \{0, \dots, M\}$ introduced above. Assume (2.1) holds and consider smooth domains, D_a', $\{W_i\}_{i=1}^M$ with $D_a' \Subset D_s$, $D_i \Subset W_i$ for $i \in \{1, \dots, M\}$. Let $B_R \Subset D_0$ and $\bigcup_{i=1}^M D_i \cup \overline{D}_s \Subset B_R$ be defined as above. In addition, assume $-k^2$ is not a Neumann eigenvalue for the Laplace operator in B_R or a Dirichlet eigenvalue for the Laplace operator in $D_{a'}$ or W_i. Let us introduce the following operator $K : L^2(\partial D_{a'}) \to L^2(\partial B_R) \times \Pi_{i=1}^M L^2(\partial W_i)$ defined by

$$(K\psi)(x) = \int_{\partial D_{a'}} \psi(\mathbf{y})\Phi(\mathbf{x}, \mathbf{y})d\mathbf{y}\ \text{ for } \mathbf{x} \text{ on } \partial B_R \times \Pi_{i=1}^M \partial W_i,$$

where $\Phi(\mathbf{x}, \mathbf{y}) = \dfrac{1}{4\pi}\dfrac{e^{ik|\mathbf{x}-\mathbf{y}|}}{|\mathbf{x}-\mathbf{y}|}$ is the 3D fundamental solution for the Helmholtz equation. Then one can characterize and compute two families of regularization parameters α_u, α_v such that the functions $u, v \in H^1(\mathbb{R}^d \setminus \overline{D}_s)$ defined by,

$$\begin{cases} u = -\mathcal{S}[(\alpha_u I + K^*K)^{-1}K^* f], \ \ f = (u_0, u_1, \dots, u_M) & \text{in } \mathbb{R}^d \setminus D_s, \\ v = -\mathcal{S}[(\alpha_v I + K^*K)^{-1}K^* g], \ \ g = (v_0, v_1, \dots, v_M) & \text{in } \mathbb{R}^d \setminus D_s, \end{cases} \tag{3.5}$$

are such that

$$\begin{cases} \Delta u + k^2 u = 0, \ \ \Delta v + k^2 v = 0 \text{ in } \mathbb{R}^d \setminus \overline{D}_s, \\ u, v \text{ satisfy the Sommerfeld radiation condition at infinity,} \\ \|u - u_0\|_{C^2(\mathbb{R}^3 \setminus D_0)} \leq \delta, \|v - v_0\|_{C^2(\mathbb{R}^3 \setminus D_0)} \leq \delta, \\ \|u - u_i\|_{C^2(D_i)} \leq \delta, \|v - v_i\|_{C^2(D_i)} \leq \delta, \end{cases} \tag{3.6}$$

where K^* denotes the adjoint of K and $\mathcal{S}$ demotes the single layer operator defined on $\partial D'_a$, i.e.,

$$(\mathcal{S}\xi)(\mathbf{x}) = \int_{\partial D_{a'}} \xi(\mathbf{y}) \Phi(\mathbf{x}, \mathbf{y}) dy \text{ for } \xi \in L^2(\partial D_{a'}).$$

We mention that the controls u, v predicted in Theorem 3.1 are explicitly constructed and can be actually computed by employing the Tikhonov regularization method together with an L-curve algorithm or the Morozov discrepancy principle to calculate the regularization parameters α_u, α_v (see [32], [53], [25]).

REMARK 3.2. We remark that similar scalar control results presented in Theorem 3.1 could also be obtained by using double layer potentials or the modified integral operators used in the literature to deal with resonant k's [13, 14].

REMARK 3.3. We remark that the sub-domain $D'_a \Subset D_s$ was introduced so that the resulting boundary data for (u, v) introduced at (3.6) (i.e., restrictions of the integral operators defined in (3.5) to ∂D_s) is smooth on the boundary of the actual physical source domain ∂D_s, since this will be desirable from the computational point of view as well as necessary for the well posedness of the exterior Maxwell boundary value problem discussed below. Also, we observe that the domains W_i with $D_i \Subset W_i$ for $i \in \{1, \ldots, M\}$ and $B_R \Subset D_0$ were used because, as it is mentioned in [52], regularity results for the interior and exterior Helmholtz problems help us get the desired C^2 estimates (3.6) in D_0, D_i from similar L^2 estimates on $\partial B_R, \partial W_i$, respectively.

The next step in our proof is to use the scalar control results presented in Theorem 3.1 and construct the necessary surface currents $\mathbf{M}$ such that the solution of (2.6) satisfies (2.7). Thus, let (u, v) be as defined in Theorem 3.1. Then, elementary algebraic manipulations and the well posedness of the exterior Maxwell problem imply that $(\mathbf{A}, \mathbf{B})$ given by

$$\mathbf{A}(\mathbf{x}) = \nabla \times (\nabla \times u\mathbf{x}) + k\nabla \times v\mathbf{x}, \ \ \mathbf{B}(\mathbf{x}) = \nabla \times (\nabla \times v\mathbf{x}) + k\nabla \times u\mathbf{x} \ \text{ in } \mathbb{R}^3 \setminus \overline{D}_s \tag{3.7}$$

are unique solutions of

$$\begin{cases} \nabla \times \mathbf{A} = k\mathbf{B}, \ \nabla \times \mathbf{B} = k\mathbf{A} & \text{in } \mathbb{R}^3 \setminus \bar{D}_s, \\ \mathbf{A} \times \mathbf{n} = (\nabla \times (\nabla \times u\mathbf{x}) + k\nabla \times v\mathbf{x}) \times \mathbf{n} & \text{on } \partial D_s, \\ (\mathbf{A}, \mathbf{B}) \text{ satisfy the Silver-Muller radiation condition at infinity,} \end{cases} \tag{3.8}$$

and based on (3.4), (3.6) we can immediately see that $(\mathbf{A}, \mathbf{B})$ satisfy

$$\begin{aligned} &\|\mathbf{A} - \mathbf{A}_0\|_{C(\mathbb{R}^3 \setminus D_0)} \leq C\delta, \quad \|\mathbf{A} - \mathbf{A}_i\|_{C(\overline{D_i})} \leq C\delta \text{ for each } i = \overline{1, M}, \\ &\|\mathbf{B} - \mathbf{B}_0\|_{C(\mathbb{R}^3 \setminus D_0)} \leq C\delta, \quad \|\mathbf{B} - \mathbf{B}_i\|_{C(\overline{D_i})} \leq C\delta \text{ for each } i = \overline{1, M} \end{aligned} \tag{3.9}$$

for some constant C. Using again the equivalence between (2.3) and (3.2) we obtain that each of the magnetic surface currents $\mathbf{M} = \frac{1}{\sqrt{-i\varepsilon\omega}}(\nabla \times (\nabla \times u\mathbf{x}) + k\nabla \times v\mathbf{x}) \times \mathbf{n}$ on ∂D_s radiates an exterior electromagnetic field $\mathbf{E}, \mathbf{H}$ with the properties that

$$\begin{aligned} &\|\mathbf{E} - \mathbf{E}_0\|_{C(\mathbb{R}^3 \setminus D_0)} \leq C\delta, \quad \|\mathbf{E} - \mathbf{E}_j\|_{C(\overline{D_j})} \leq C\delta \text{ for each } j = \overline{1, M}, \\ &\|\mathbf{H} - \mathbf{H}_0\|_{C(\mathbb{R}^3 \setminus D_0)} \leq C\delta, \quad \|\mathbf{H} - \mathbf{H}_j\|_{C(\overline{D_j})} \leq C\delta \text{ for each } j = \overline{1, M}, \end{aligned} \tag{3.10}$$

where the constant C depends only on ω, ε, μ. □

REMARK 3.4. The above proof can be immediately adapted to show that, in the same conditions as in Theorem 2.1, one can characterize conduction currents $\mathbf{J} = \mathbf{H} \times \mathbf{n}$ such that (2.6), (2.7) hold true.

REMARK 3.5. Note that from the physical point of view, the instantiation of magnetic surface currents $\mathbf{M} = \mathbf{E} \times \mathbf{n}$ or conduction surface currents $\mathbf{J} = \mathbf{H} \times \mathbf{n}$ on the source region ∂D_s will correspond to a Perfect Magnetic Conductor (PMC) or, respectively, a Perfect Electric Conductor (PEC) in D_s.

First strategy for the computation of the surface currents. The proof of Theorem 2.1 presented above suggests the first scheme for the computation of the surface currents required on the boundary of the source ∂D_s:

1. Use the given electromagnetic fields $(\mathbf{E}_i, \mathbf{H}_i)$ in source free regions Σ_i and (3.3) to compute their respective scalar Debye potentials (u_i, v_i) for each $i = \overline{0, M}$ (see (3.4)). Alternatively, one could consider spherical harmonics approximation of $(\mathbf{E}_i, \mathbf{H}_i)$ on annular regions Σ_i, and by using the fact that for each $i = \overline{0, M}$ we have $\Delta_{B_r} u_i = -r\mathbf{E}_i \cdot \hat{\mathbf{r}}, \Delta_{B_r} v_i = -r\mathbf{H}_i \cdot \hat{\mathbf{r}}$ for each r with $(r, \theta, \varphi) \in \Sigma_i$ (where $\hat{\mathbf{r}}$ has been defined in (3.3) and Δ_{B_r} denotes the Laplace-Beltrami operator on the sphere ∂B_r) and that spherical harmonics are eigenfunctions of Δ_{B_r} obtain another computational avenue for (u_i, v_i) for each $i = \overline{0, M}$.

2. Employ the computed (u_i, v_i) for each $i = \overline{0, M}$ to solve the two scalar inverse problems and find the scalar potentials (u, v) as in (3.5).

3. Use the properties of spherical harmonics in (3.7) (employing the equivalence between (2.3) and (3.2)) to explicitly compute the radiated electromagnetic field $(\mathbf{E}, \mathbf{H})$ corresponding to the computed scalar potentials (u, v). The desired surface magnetic current (or conduction current) required on the surface is given then by $\mathbf{E} \times \mathbf{n}$ (or $\mathbf{H} \times \mathbf{n}$) on ∂D_s.

As mentioned in Remark 3.5 the above analysis considers only the case when the source D_s is filled with a PEC or PMC material and thus supports only one type of surface current, conduction current or magnetic current, respectively. Theorem 2.1 states the existence of magnetic or conduction surface currents so that the resulting radiated electromagnetic fields will satisfy (2.6), (2.7) and it also reveals a potential way to construct and compute these boundary currents by making use of the scalar control results of Theorem 3.1. We remark that due to the presence of the highly numerically unstable operators $\nabla\times$ and $\nabla \times \nabla\times$ in this scheme, its computational feasibility requires the use of a global basis expansion (e.g., spherical harmonics) for the unknown surface densities (dipole moments) so that the differential expression can be analytically computed before the assembly of the moment matrix.

Second strategy for the computation of the surface currents. In what follows we present our second approach for the characterization and calculation of the required surface currents in Theorem 2.1. This approach, while providing another strategy for the computation of the surface currents predicted by Theorem 2.1 above will also apply to the general case of sources D_s supporting magnetic as well as conduction surface currents (where non-trivial interior fields will also exist inside D_s), and will be a stepping stone towards the case of disconnected source regions, (i.e., arrays or swarms).

Following [7, Section 2.10], we introduce the electromagnetic field $(\mathbf{E}_m, \mathbf{H}_m)$ (solution of (2.3)) generated by a magnetic ideal dipole with dipole moment $a \in \mathbb{R}^3$ and located at point $\mathbf{y} \in \mathbb{R}^3$ as

$$\mathbf{E}_m(\mathbf{x}) = i\omega\mu\nabla_x \times (a\Phi(\mathbf{x},\mathbf{y})),\ \mathbf{H}_m(\mathbf{x}) = \frac{1}{i\omega\mu}\nabla_x \times \mathbf{E}_m(\mathbf{x}), x \in \mathbb{R}^3 \setminus \{y\}, \tag{3.11}$$

and the electromagnetic field $(\mathbf{E}_e, \mathbf{H}_e)$ generated by an electric ideal dipole with dipole moment $a \in \mathbb{R}^3$ and located at point $\mathbf{y} \in \mathbb{R}^3$ as

$$\mathbf{H}_e(\mathbf{x}) = \nabla_x \times (a\Phi(\mathbf{x},\mathbf{y})),\ \mathbf{E}_e(\mathbf{x}) = -\frac{1}{i\omega\varepsilon}\nabla_x \times \mathbf{H}_e(\mathbf{x}), x \in \mathbb{R}^3 \setminus \{y\}. \tag{3.12}$$

Next, we also recall two fundamental electromagnetic representation results [13, Section 4.2] (see also [22]).

THEOREM 3.6 ([13]). Let $D \Subset \mathbb{R}^3$ be a bounded open connected domain. Then,

1. If $(\mathbf{E}, \mathbf{H}) \in C^1(\mathbb{R}^3 \setminus \overline{D}) \cap C(\mathbb{R}^3 \setminus D)$ is a solution of Maxwell's equations (2.3) in $\mathbb{R}^3 \setminus \overline{D}$ satisfying the Silver-Muller radiation condition at infinity we have

$$\nabla \times \int_{\partial D} (\mathbf{n}(\mathbf{y}) \times \mathbf{E}(\mathbf{y}))\Phi(\mathbf{x},\mathbf{y}) - \frac{\sqrt{\mu}}{ik\sqrt{\varepsilon}}\nabla \times \nabla \times \int_{\partial D} (\mathbf{n}(\mathbf{y}) \times \mathbf{H}(\mathbf{y}))\Phi(\mathbf{x},\mathbf{y}) = \begin{cases} 0, & \mathbf{x} \in D, \\ \mathbf{E}(\mathbf{x}), & \mathbf{x} \in \mathbb{R}^3 \setminus \overline{D}, \end{cases} \tag{3.13}$$

and

$$\nabla \times \int_{\partial D} (\mathbf{n}(\mathbf{y}) \times \mathbf{H}(\mathbf{y}))\Phi(\mathbf{x},\mathbf{y})ds(\mathbf{y}) + \frac{\sqrt{\varepsilon}}{ik\sqrt{\mu}}\nabla \times \nabla \times \int_{\partial D} (\mathbf{n}(\mathbf{y}) \times \mathbf{E}(\mathbf{y}))\Phi(\mathbf{x},\mathbf{y})ds(\mathbf{y}) = \begin{cases} 0, & \mathbf{x} \in D, \\ \mathbf{H}(\mathbf{x}), & \mathbf{x} \in \mathbb{R}^3 \setminus \overline{D}. \end{cases} \tag{3.14}$$

2. If $(\mathbf{E}, \mathbf{H}) \in C^1(D) \cap C(\overline{D})$ is a solution of Maxwell's equations (2.3) in D, then

$$\nabla \times \int_{\partial D} (\mathbf{n}(\mathbf{y}) \times \mathbf{E}(\mathbf{y}))\Phi(\mathbf{x},\mathbf{y})ds(\mathbf{y}) - \frac{\sqrt{\mu}}{ik\sqrt{\varepsilon}}\nabla \times \nabla \times \int_{\partial D} (\mathbf{n}(\mathbf{y}) \times \mathbf{H}(\mathbf{y}))\Phi(\mathbf{x},\mathbf{y})ds(\mathbf{y}) = \begin{cases} -\mathbf{E}(\mathbf{x}), & \mathbf{x} \in D, \\ 0, & \mathbf{x} \in \mathbb{R}^3 \setminus \overline{D}, \end{cases} \tag{3.15}$$

and

$$\nabla \times \int_{\partial D} (\mathbf{n}(\mathbf{y}) \times \mathbf{H}(\mathbf{y}))\Phi(\mathbf{x},\mathbf{y})ds(\mathbf{y}) \\ + \frac{\sqrt{\varepsilon}}{ik\sqrt{\mu}}\nabla \times \nabla \times \int_{\partial D} (\mathbf{n}(\mathbf{y}) \times \mathbf{E}(\mathbf{y}))\Phi(\mathbf{x},\mathbf{y})ds(\mathbf{y}) = \begin{cases} -\mathbf{H}(\mathbf{x}), & \mathbf{x} \in D, \\ 0, & \mathbf{x} \in \mathbb{R}^3 \setminus \overline{D}. \end{cases} \tag{3.16}$$

Theorem 2.1, implies that the electromagnetic fields $(\mathbf{E}, \mathbf{H})$ given by

$$\mathbf{E}(\mathbf{x}) = \frac{1}{\sqrt{-i\varepsilon\omega}}(\nabla \times (\nabla \times u\mathbf{x}) + k\nabla \times v\mathbf{x}), \\ \mathbf{H}(\mathbf{x}) = \frac{1}{\sqrt{i\mu\omega}}(\nabla \times (\nabla \times v\mathbf{x}) + k\nabla \times u\mathbf{x}), \tag{3.17}$$

with Helmholtz potentials u, v defined at (3.6), has the property that $(\mathbf{E}, \mathbf{H}) \in C^1(\mathbb{R}^3 \setminus \overline{D}) \cap C(\mathbb{R}^3 \setminus D)$ and is a radiating solution of Maxwell's equation in $\mathbb{R}^3 \setminus D$ satisfying inequalities (2.7). Then, for general source domains D_s not necessarily PMC or PEC, (3.11) and (3.12) used in (3.13), (3.14) of Theorem 3.6 with $D = D_s$ imply that, in principle, one can characterize a layer of electric and magnetic tangential dipoles with dipole density proportional to $\mathbf{n}(\mathbf{y}) \times \mathbf{H}(\mathbf{y})$ and, respectively, $\mathbf{n}(\mathbf{y}) \times \mathbf{E}(\mathbf{y})$ distributed on ∂D_s so that the field generated by it will be zero in D_s while being equal $(\mathbf{E}, \mathbf{H})$ in $\mathbb{R}^3 \setminus D$ thus having the desired properties as in (2.7). In particular, if D_s is a PMC material, then Theorem 3.6 gives

$$\nabla \times \textstyle\int_{\partial D} (\mathbf{n}(\mathbf{y}) \times \mathbf{E}_g(\mathbf{y}))\Phi(\mathbf{x},\mathbf{y}) = \begin{cases} 0, & \mathbf{x} \in D_s, \\ \mathbf{E}_g(\mathbf{x}), & \mathbf{x} \in \mathbb{R}^3 \setminus \overline{D}_s, \end{cases} \tag{3.18}$$

$$\tfrac{\sqrt{\varepsilon}}{ik\sqrt{\mu}}\nabla \times \nabla \times \textstyle\int_{\partial D_s} (\mathbf{n}(\mathbf{y}) \times \mathbf{E}_g(\mathbf{y}))\Phi(\mathbf{x},\mathbf{y})ds(\mathbf{y}) = \begin{cases} 0, & \mathbf{x} \in D_s, \\ \mathbf{H}_g(\mathbf{x}), & \mathbf{x} \in \mathbb{R}^3 \setminus \overline{D}_s, \end{cases}$$

and a similar simplification will hold for the case when D_s is a PEC. This result theoretically validates a second alternative scheme for the computation of the surface currents predicted in Theorem 2.1 which will be based on solving a system of ill-posed associated integral equations of the first kind as suggested by (3.18). That is, in the particular case for instance of a PMC material in D_s, for given $(\mathbf{E}_0, \mathbf{H}_0)$ and $(\mathbf{E}_i, \mathbf{H}_i)$, with $1 \leq i \leq M$ as in Theorem 2.1, the scheme requires us to solve for the smooth tangential vector densities $\mathbf{w}_e$ in the following ill posed system:

$$\begin{aligned} \nabla \times \int_{\partial D} \mathbf{w}_e(\mathbf{y})\Phi(\mathbf{x},\mathbf{y}) &= \mathbf{E}_i(\mathbf{x}) \text{ in } D_i, \\ \nabla \times \int_{\partial D} \mathbf{w}_e(\mathbf{y})\Phi(\mathbf{x},\mathbf{y}) &= \mathbf{E}_0(\mathbf{x}) \text{ on } \partial D_0, \end{aligned} \tag{3.19}$$

where the well posedness of the exterior Maxwell problem was used to justify the sufficiency of the second equation. We remark that multiple discretization approaches either in the spirit of [22] or employing various local basis approximations can be used for this scheme so that a matrix of moments can be feasibly computed and the resulting linear system efficiently solved.

Note that due to analytic continuation there exists no exact solution for the system (3.19) but an infinity of approximate solutions with asymptotically small residuals exist as guaranteed by (3.18). By using the fact that $(\mathbf{E}_0, \mathbf{H}_0)$ and $(\mathbf{E}_i, \mathbf{H}_i)$, with $1 \leq i \leq M$ are solutions of the Maxwell system in regions $\mathbb{R}^3 \setminus D_0, D_i$, respectively, a good approximate solution of (3.19) should imply the accurate approximations of the magnetic fields,

$$\begin{aligned} \frac{1}{i\omega\mu}\nabla\times\nabla\times\int_{\partial D}\mathbf{w}_e(\mathbf{y})\Phi(\mathbf{x},\mathbf{y})ds(\mathbf{y}) &= \mathbf{H}_0(\mathbf{x}) \text{ in } \mathbb{R}^3\setminus D_0, \\ \frac{1}{i\omega\mu}\nabla\times\nabla\times\int_{\partial D}\mathbf{w}_e(\mathbf{y})\Phi(\mathbf{x},\mathbf{y})ds(\mathbf{y}) &= \mathbf{H}_i(\mathbf{x}) \text{ in } D_i \text{ for } i\in\{1,M\}. \end{aligned} \tag{3.20}$$

4. Numerical framework. In this section, we will focus on the first solution strategy for Theorem 2.1 discussed above and present the framework for the design of a computationally feasible numerical scheme implementing the theoretical results presented in this approach. As discussed above this scheme involves three major steps. First, the prescribed electric and magnetic fields will be expressed in terms of Debye potentials. Thus, the original vectorial Maxwell system will be "replaced" by a pair of scalar Helmholtz problems. Then the second step of this scheme requires the solution of the two associated scalar Helmholtz inverse problems using the method proposed in [52], [53], and [25]. The last component represents the computation of the radiated electric and magnetic fields corresponding to the pair of Debye potentials obtained in the second component. These potentials also give the required boundary current solving the main problems (2.6)-(2.7). One major challenge in this strategy is the calculation of the curls and curl-curls in (3.7). Numerical approximations of curls and curl-curls are very unstable and may introduce errors that will be propagated along the process. To avoid this situation, we will use global basis functions for the expansion of our unknown scalar densities such that the curl and curl-curls of the moments can be a priori explicitly computed.

4.1. *Debye potential representation of the EM field.* Recall that the problem of finding a boundary current $\mathbf{M}$ such that the electric and magnetic fields $\mathbf{E}$ and $\mathbf{H}$ satisfy (2.6) and (2.7) can be reformulated in the Wilcox paradigm as

$$\begin{cases} \nabla\times\mathbf{A} &= k\mathbf{B}, \\ \nabla\times\mathbf{B} &= k\mathbf{A}. \end{cases} \tag{4.1}$$

Then the vector fields in (4.1) can be expressed as

$$\begin{cases} \mathbf{A}(\mathbf{r}) &= \nabla\times(\nabla\times u\mathbf{r}) + k\nabla\times v\mathbf{r} \text{ and} \\ \mathbf{B}(\mathbf{r}) &= \nabla\times(\nabla\times v\mathbf{r}) + k\nabla\times u\mathbf{r} \end{cases} \tag{4.2}$$

for some scalar fields u and v satisfying (3.6). Further, given the prescribed fields $\mathbf{A}_p$ and $\mathbf{B}_p$, the corresponding scalar fields u_p and v_p can be computed as the integrals

$$\begin{aligned} u_p(r\hat{\mathbf{r}}) &= -\frac{r}{2\pi}\int_{B_1}\left(\log(\sin\frac{\gamma}{2})\right)\hat{\mathbf{r}}\cdot\mathbf{A}_p(r\hat{\mathbf{r}'})d\sigma' \text{ and} \\ v_p(r\hat{\mathbf{r}}) &= -\frac{r}{2\pi}\int_{B_1}\left(\log(\sin\frac{\gamma}{2})\right)\hat{\mathbf{r}}\cdot\mathbf{B}_p(r\hat{\mathbf{r}'})d\sigma'. \end{aligned} \tag{4.3}$$

Let $B_{r_0} = D'_a \Subset D_s$ as in Section 2. As shown in [25], there exists fields u and v such that

$$\begin{cases} \Delta u + k^2 u = 0, \ \ \Delta v + k^2 v = 0 \text{ in } \mathbb{R}^d \setminus \overline{D}_s, \\ u, v \text{ satisfy the Sommerfeld radiation condition at infinity,} \\ \|u - u_p\|_{C^2(D)} \leq \delta, \|v - v_p\|_{C^2(D)} \leq \delta \end{cases} \tag{4.4}$$

for any collection of control regions D and preset accuracy threshold δ. Moreover, the fields u and v can be approximated using densities w_u and w_v on D'_a given by the truncated series

$$w_u(\mathbf{y}) = \sum_{l=0}^{L} \sum_{p=-l}^{l} \alpha_{pl} Y_l^p(\hat{\mathbf{y}}) \text{ and} \tag{4.5}$$

$$w_v(\mathbf{y}) = \sum_{l=0}^{L} \sum_{p=-l}^{l} \beta_{pl} Y_l^p(\hat{\mathbf{y}}), \tag{4.6}$$

where Y_l^p is the orthonormal family of spherical harmonics as considered in ([14, Chapter 2], [1]). Then using the addition theorem and the orthogonality of spherical harmonics in (3.5), u and v can be approximated by the following truncated series of spherical Hankel functions $h_n^{(1)}$ of the first kind and spherical Bessel functions j_n of order n:

$$u(r,\theta,\phi) \approx u_g(r,\theta,\phi) = ikr_0^2 \sum_{l=0}^{L} \sum_{p=-l}^{l} \alpha_{pl} \ j_l(kr_0) \ h_l^{(1)}(kr) \ Y_l^p(\theta,\phi) \text{ and} \tag{4.7}$$

$$v(r,\theta,\phi) \approx v_g(r,\theta,\phi) = ikr_0^2 \sum_{l=0}^{L} \sum_{p=-l}^{l} \beta_{pl} \ j_l(kr_0) \ h_l^{(1)}(kr) \ Y_l^p(\theta,\phi), \tag{4.8}$$

where r_0 is again the radius of the spherical fictitious source. The set of coefficients α_{pl} and β_{pl} are then computed following the numerical scheme in [53] and [25] which uses Tikhonov regularization with the Morozov discrepancy principle.

4.2. *Calculating the surface current and the generated EM fields.* The use of spherical harmonics in solving the scalar problems (4.4) provided a truncated series representation for the generated fields u_g and v_g. These representations are better suited for a numerical implementation instead of the integral operator forms suggested in (3.5). Moreover, we shall see in the following discussions that the spherical harmonic decomposition will provide an analytic expression for the curls and curl-curls required in (4.2).

Let w be a scalar Debye potential. In spherical coordinates, it can be shown that

$$\nabla \times w\mathbf{r} = \left\langle 0, \frac{1}{\sin\theta} \frac{\partial w}{\partial \phi}, -\frac{\partial w}{\partial \theta} \right\rangle \tag{4.9}$$

and that $\nabla \times \nabla \times w\mathbf{r}$ has r, θ and ϕ components given by

$$\begin{aligned} (\nabla \times \nabla \times w\mathbf{r})_r &= \frac{1}{r\sin\theta} \left(-\frac{\partial^2 w}{\partial \theta^2} \sin\theta - \frac{\partial w}{\partial \theta} \cos\theta - \frac{1}{\sin\theta} \frac{\partial^2 w}{\partial \phi^2} \right), \\ (\nabla \times \nabla \times w\mathbf{r})_\theta &= \frac{1}{r} \left(\frac{\partial w}{\partial \theta} + r \frac{\partial^2 w}{\partial r \partial \theta} \right), \\ (\nabla \times \nabla \times w\mathbf{r})_\phi &= \frac{1}{r\sin\theta} \left(\frac{\partial w}{\partial \phi} + r \frac{\partial^2 w}{\partial r \partial \phi} \right), \end{aligned} \tag{4.10}$$

respectively. Then to compute the generated fields $\mathbf{A}_g$ and $\mathbf{B}_g$ via the relations in (4.2), we can use the series representation of u_g and v_g given at (4.7), (4.8) in the curl and curl-curl formulas (4.9), (4.10). To avoid numerical errors and computational instability, the curl and curl-curl of u_g and v_g will be calculated exactly. Calculating the derivatives of the spherical harmonics Y_l^p is straightforward, while the derivative of the spherical Hankel and spherical Bessel functions are given by the recurrence relations:

$$\frac{\partial h_n^{(1)}}{\partial r}(r) = \begin{cases} -h_1^{(1)}(r), & n = 0, \\ \dfrac{1}{2}\left[h_{n-1}^{(1)}(r) - \dfrac{1}{r}h_n^{(1)}(r) - h_{n+1}^{(1)}(r)\right], & n > 0, \end{cases} \tag{4.11}$$

and

$$\frac{\partial j_n}{\partial r}(r) = \begin{cases} -j_1(r), & n = 0, \\ \dfrac{1}{2}\left[j_{n-1}(r) - \dfrac{1}{r}j_n(r) - j_{n+1}(r)\right], & n > 0. \end{cases} \tag{4.12}$$

With these identities and the series expansions (4.7) and (4.8) plugged in (4.2), the generated fields $(\mathbf{A}_g, \mathbf{B}_g)$ can be obtained analytically, thereby avoiding the instability of numerical approximations to the curl operator. This leads to an accurate calculation of the required magnetic surface current $\mathbf{M}$ on ∂D_s:

$$\mathbf{M}(\mathbf{r}) = \mathbf{A}_g(\mathbf{r}) \times \mathbf{n} = (\nabla \times (\nabla \times u_g \mathbf{r}) + k\nabla \times v_g \mathbf{r}) \times \mathbf{n}. \tag{4.13}$$

Then with the appropriate conversion between the two equivalent forms of the Maxwell system (2.3) and (3.2), $\mathbf{E}$ and $\mathbf{H}$ can be obtained.

5. Numerical results. In this section, we present several numerical results supporting the analysis presented in the preceding sections. We consider three geometric configurations namely, single region synthesis, double region synthesis, and the case of an almost non-radiating source. In all these cases the wave number is $k = 1$. The electromagnetic fields are approximated using 70 harmonic orders resulting to a total of 5041 unknown coefficients. The physical source is the sphere $B_{0.0105}(\mathbf{0})$ while the fictitious source is the smaller sphere $B_{0.01}(\mathbf{0})$ modeled by a 200×100 $\theta\phi$-mesh. However, note that the physical source may assume any shape with Lipschitz continuous boundary as long as it contains the fictitious source and satisfies the separation properties introduced at (2.1). The near control region D_1 is always the annular sector

$$D_1 = \left\{(r, \theta, \phi) : r \in [0.012, 0.016], \theta \in \left[\frac{\pi}{4}, \frac{3\pi}{4}\right], \phi \in \left[\frac{3\pi}{4}, \frac{5\pi}{4}\right]\right\}. \tag{5.1}$$

For the numerics, D_1 is discretized into 37800 collocation points. In all of the three simulations below, we prescribe on D_1 the electric field $\mathbf{E}(\mathbf{r}) = \mathbf{E}_0 e^{i\mathbf{k}\cdot\mathbf{r}}$ where $\mathbf{E}_0 = \langle 0, 1, 0\rangle$ and $\mathbf{k} = k\langle -1, 0, 0\rangle$ in Cartesian coordinates and its corresponding magnetic field $\mathbf{H}(\mathbf{r}) = \mathbf{k} \times \mathbf{E}(\mathbf{r})$. The control region D_2 is either the annular sector

$$D_2 = \left\{(r, \theta, \phi) : r \in [0.012, 0.016], \theta \in \left[\frac{\pi}{4}, \frac{3\pi}{4}\right], \phi \in \left[0, \frac{\pi}{4}\right] \cup \left[\frac{7\pi}{4}, 2\pi\right]\right\} + (0.1, 0, 0) \tag{5.2}$$

for the double region synthesis or the unbounded region $D_2 = \mathbb{R}^3 \setminus B_{10}(\mathbf{0})$ for the case of an almost non-radiating source.

We measure the accuracy of our solution by looking at several indicators. In each experiment, we present a visual comparison between the three components (r, θ, and ϕ) of the prescribed and generated electric and magnetic fields. Whenever a component of the prescribed field is non-zero everywhere on the control region(s), we calculate and plot the relative error at each point on the control. We also calculate the L^2 relative error as a global measure of accuracy. For the radial component, we compute the L^2 relative error as $\frac{\|\mathbf{E}_{p,r} - \mathbf{E}_{g,r}\|_2}{\|\mathbf{E}_{p,r}\|_2}$ for the electric field and $\frac{\|\mathbf{H}_{p,r} - \mathbf{H}_{g,r}\|_2}{\|\mathbf{H}_{p,r}\|_2}$ for the magnetic field provided $\|\mathbf{E}_{p,r}\|_2 \neq 0$, $\|\mathbf{H}_{p,r}\|_2 \neq 0$ and where $\mathbf{E}_{p,r}$ and $\mathbf{E}_{g,r}$ are the radial components of the prescribed and generated electric fields, respectively. Analogous formulas for the fields' θ and ϕ components are used.

5.1. *Single region field synthesis.* In this simulation, we consider a single control region: the annular sector

$$D_1 = \left\{ (r, \theta, \phi) : r \in [0.012, 0.016], \theta \in \left[\frac{\pi}{4}, \frac{3\pi}{4}\right], \phi \in \left[\frac{3\pi}{4}, \frac{5\pi}{4}\right] \right\}.$$

In this region we prescribe the electromagnetic wave traveling in the direction of the negative x-axis as described above. The top view of the problem geometry is sketched in Figure 2.

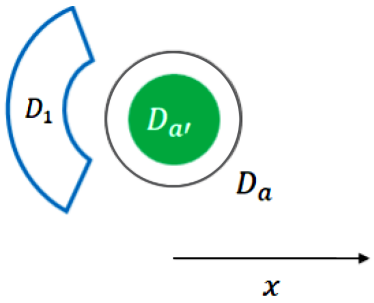

FIG. 2. Sketch of the problem geometry for the case of a single region field synthesis

Figure 3 shows a visual comparison between the three components of the prescribed electric field (top row) and the corresponding components of the generated electric field (bottom row). The plots indicate a good approximation of all three components of the prescribed field. The good visual match is confirmed in Figure 4 where the pointwise relative errors for all of the field's components are shown. Note that at some points in the control region, the values to be matched, specifically for the radial and the θ-components are close to zero, causing the relative error to show very large values. This can be observed as the bright stripes in plots (A) and (B) of Figure 4. However, the overall L^2-relative errors are small, with values of about 1.59×10^{-2}, 1.84×10^{-2}, and 5.56×10^{-3} for the r-, θ-, and ϕ-components, respectively.

Similar good results are also obtained for the magnetic fields. The components of the prescribed and generated fields are shown in Figure 5. Note that the prescribed magnetic field has a zero ϕ-component everywhere. It can be observed from the plots that the radial and θ-components are matched very well, except for some spots near

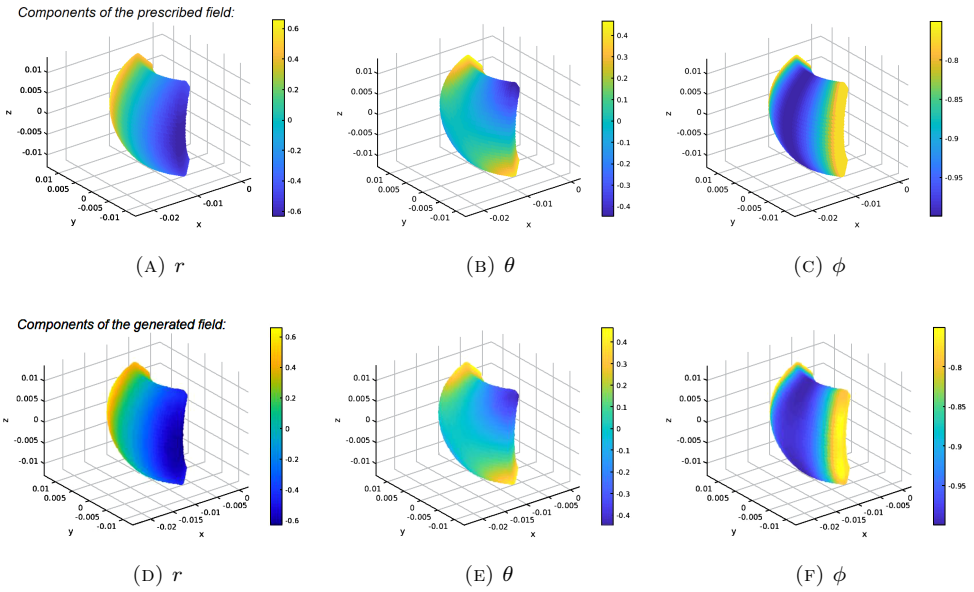

(A) r (B) θ (C) ϕ

(D) r (E) θ (F) ϕ

FIG. 3. Results of the electric field synthesis on D_1

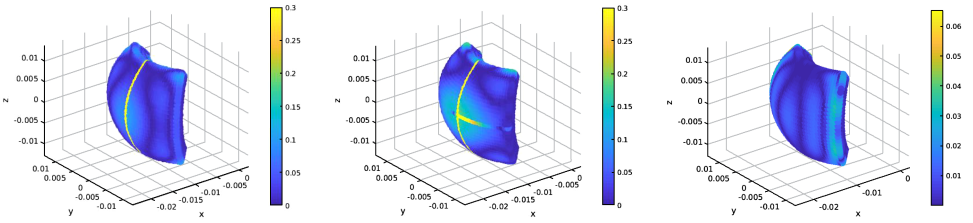

(A) r (B) θ (C) ϕ

FIG. 4. Plots of the pointwise relative errors of the electric field on D_1

the top edge of the region. The generated magnetic field's ϕ-components are small with values of order 10^{-5}.

The pointwise relative errors for the r- and θ-components of the generated magnetic fields are shown in Figure 6. The pointwise relative errors for both components are within desirable levels, except for some isolated points where the errors exceed 20. The overall L^2 relative errors are about 1.70×10^{-2} and 7.66×10^{-3} for the r- and θ-components, respectively. The L^2 norm of the generated magnetic field's ϕ-component is just around 7.48×10^{-6}.

The complex current used to generate the results above is described in the plots shown in Figure 7. This figure includes three two-dimensional plots in the θ-ϕ plane: (A) a color map of the current's magnitude and the quiver plots of the current's (B) real and (C) imaginary parts. It can be noted that there are points on the source where the current has magnitude above 3.5×10^4.

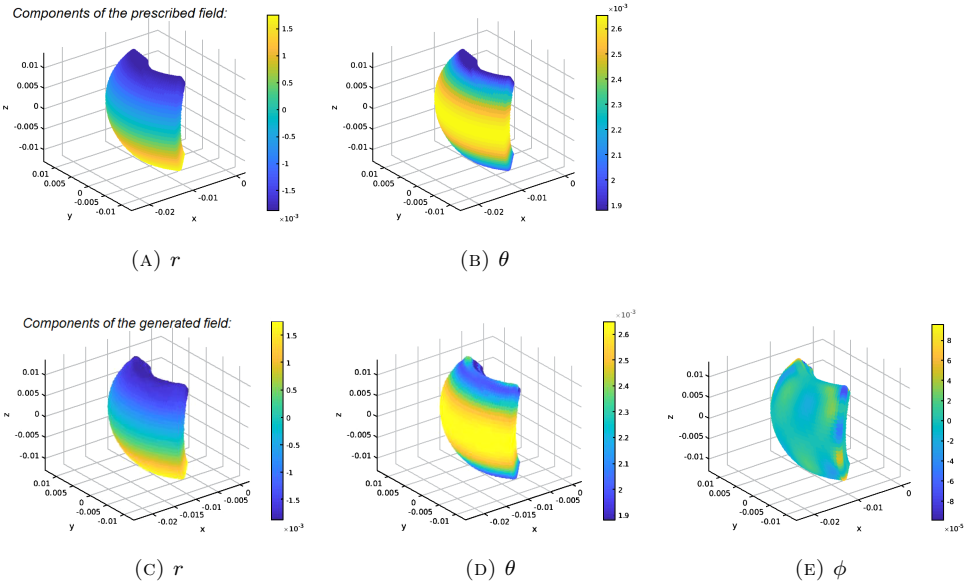

(A) r (B) θ

(C) r (D) θ (E) ϕ

FIG. 5. Results of the magnetic field synthesis on D_1

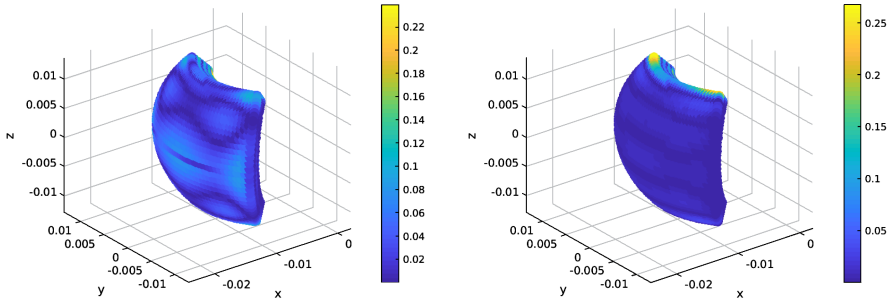

(A) r-component (B) θ-component

FIG. 6. Plots of the pointwise relative errors of the magnetic field on D_1

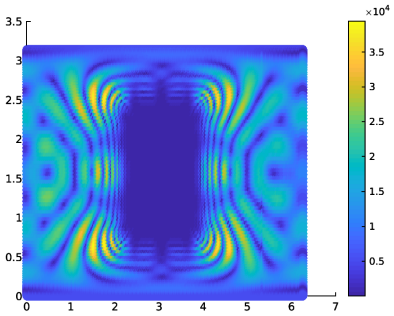

(A) Magnitude

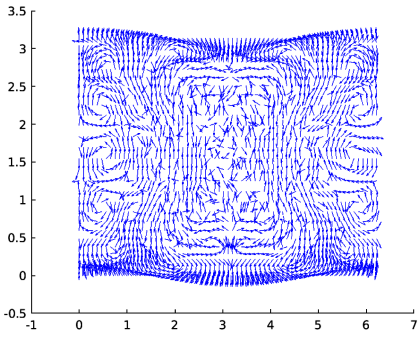

(B) Real part

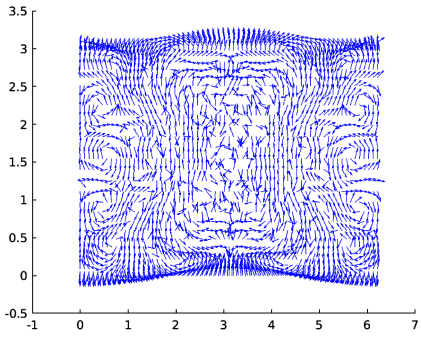

(C) Imaginary part

FIG. 7. Plot of the calculated complex current's magnitude and quiver plots of its real and imaginary parts

5.2. *Double region field synthesis.* In the following simulation, we consider two annular sectors as control regions, the near control

$$D_1 = \left\{ (r, \theta, \phi) : r \in [0.012, 0.016], \theta \in \left[\frac{\pi}{4}, \frac{3\pi}{4} \right], \phi \in \left[\frac{3\pi}{4}, \frac{5\pi}{4} \right] \right\}$$

and the far control

$$D_2 = \left\{ (r, \theta, \phi) : r \in [0.012, 0.016], \theta \in \left[\frac{\pi}{4}, \frac{3\pi}{4} \right], \phi \in \left[0, \frac{\pi}{4} \right] \cup \left[\frac{7\pi}{4}, 2\pi \right] \right\} + (0.1, 0, 0).$$

The near control is discretized into 37800 collocation points while the far control is modeled by a mesh of 25600 points. In D_1 we prescribe the left traveling electromagnetic plane wave described above while in D_2 we approximate a null field. The problem geometry is sketched in Figure 8.

A visual comparison of the prescribed (top row) and generated (bottom row) electric fields is given in Figure 9. The plots suggest a good match for the radial component all throughout D_1. The θ-component is also matched well except for some patch near the control's upper left edge. Meanwhile, there are some noticeable differences in the ϕ-component in some patches near the region's left and right edges. The pointwise relative

errors for each component of the generated electric field is shown in Figure 10. Again, there are some points where the relative error may seem to blow up. These are the points where the field component is exactly or is close to zero. The overall L^2 relative error for each component suggests a good approximation of the prescribed fields. The values are about 3.52×10^{-2}, 5.34×10^{-2}, and 1.13×10^{-2} for the r, θ, and ϕ components, respectively.

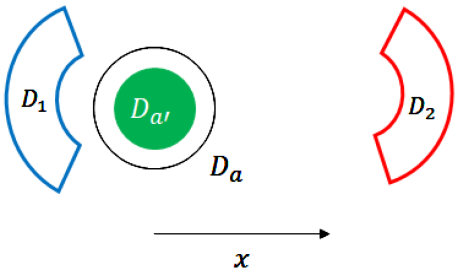

FIG. 8. Sketch of the problem geometry for the case of a double region field synthesis

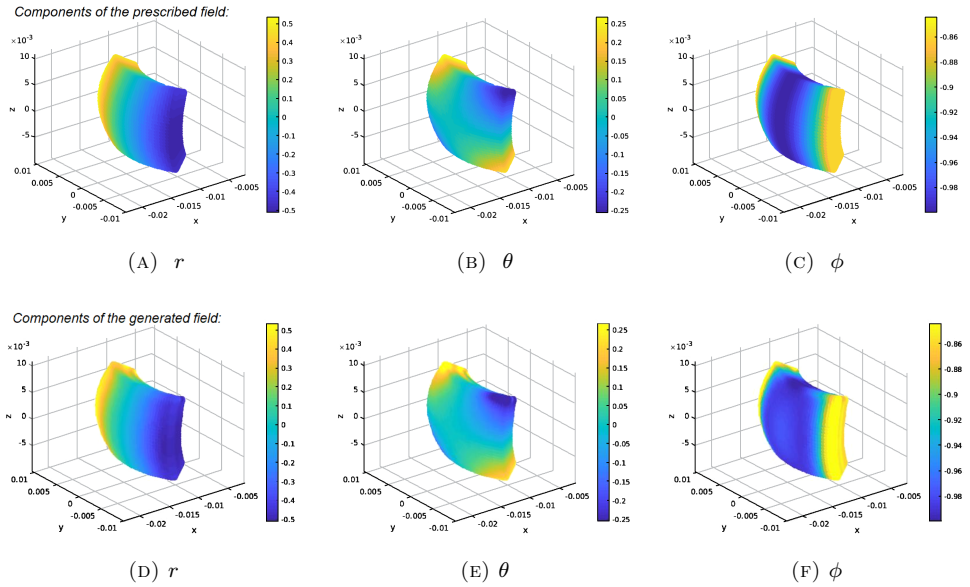

(A) r (B) θ (C) ϕ

(D) r (E) θ (F) ϕ

FIG. 9. Results of the electric field synthesis on D_1

The results of the simulation for the magnetic field on the near control D_1 are shown in Figure 11. In the said figure, the three components of the prescribed and generated fields are shown. Again note that the ϕ-component of the magnetic field is zero in D_1. From these plots, it can be inferred that the synthesis of the prescribed pattern generally went well, though there were patches near the top edge of the region where there are

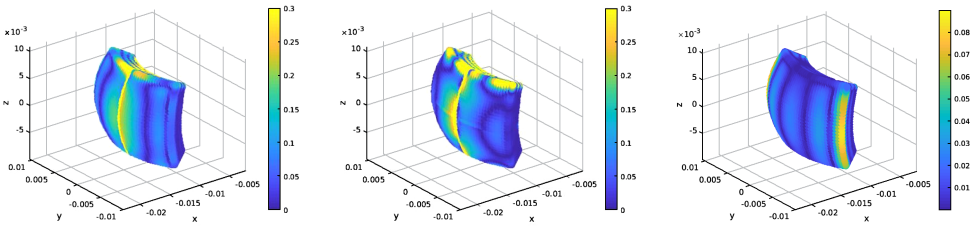

(A) r (B) θ (C) ϕ

FIG. 10. Plots of the pointwise relative errors of the electric field on D_1

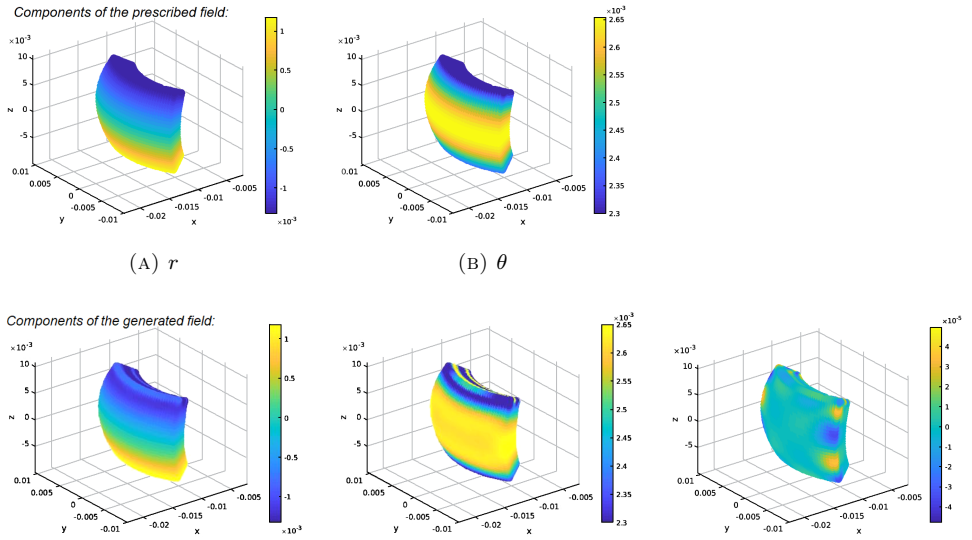

(A) r (B) θ

(C) r (D) θ (E) ϕ

FIG. 11. Results of the magnetic field synthesis on D_1

noticeable differences in the r- and θ-components of the two fields. The generated field has a very low ϕ-component as desired: with values of order 10^{-5}.

The pointwise relative error for the r- and θ-components of the magnetic field are shown in Figure 12. Indeed, the relative errors are highest on the top of the region. However, the L^2 relative error for both components are within desired levels, with values of around 5.58×10^{-2} and 1.44×10^{-2} for the r- and θ-components, respectively. The L^2 norm of the field's ϕ-component is very small at about 4.87×10^{-6}.

Now we look at the results for the control region D_2. Figure 13 shows the generated electric field on D_2. All three components have low magnitudes, with supremum absolute values of 8.25×10^{-4}, 1.03×10^{-3}, and 8.28×10^{-3} for the r-, θ-, ϕ-components, respectively. The overall L^2 norms of the generated field for each component are 4.93×10^{-4}, 2.86×10^{-4}, and 7.74×10^{-3}, in the same order.

A very low magnetic field on D_2 was generated. Figure 14 shows the plot of all three components of this field. The supremum of the r-, θ- and ϕ-components on D_2 are 3.18×10^{-6}, 9.09×10^{-6}, and 1.22×10^{-6}, and their L^2 norms are 1.45×10^{-6}, 8.57×10^{-6}, and 3.47×10^{-7}, respectively.

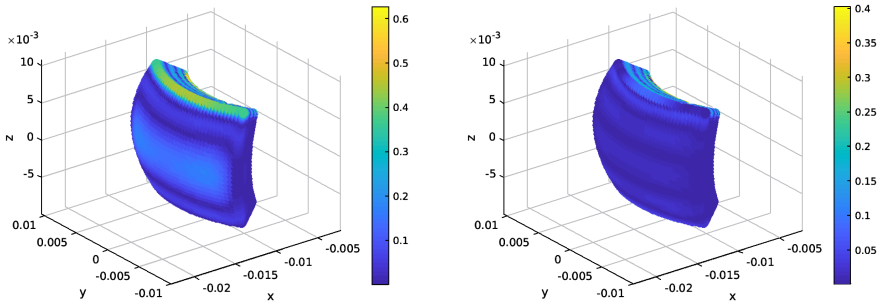

(A) r-component (B) θ-component

FIG. 12. Plots of the pointwise relative errors of the magnetic field on D_1

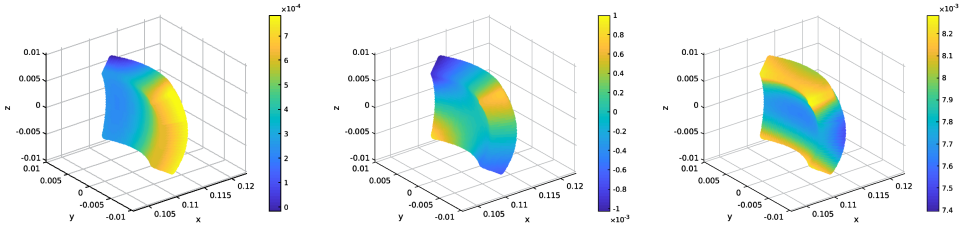

(A) r (B) θ (C) ϕ

FIG. 13. Components of the generated electric field on D_2

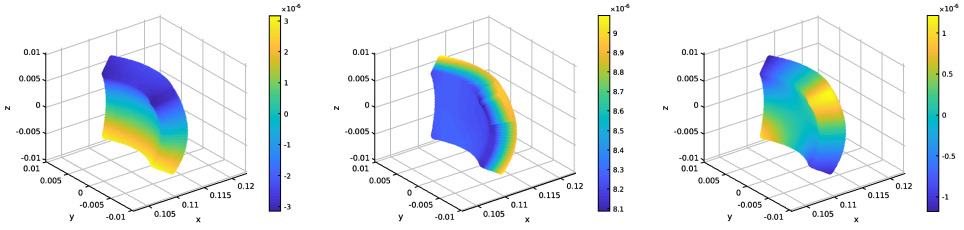

(A) r (B) θ (C) ϕ

FIG. 14. Components of the generated magnetic field on D_2

The calculated current used to generate the fields described above is characterized in Figure 15 using three $\theta\phi$-rectangular plots, similar to the previous simulation. It can be noted that the current's complex magnitude reaches values of order 10^4.

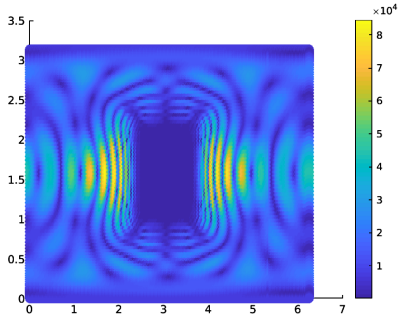

(A) Magnitude

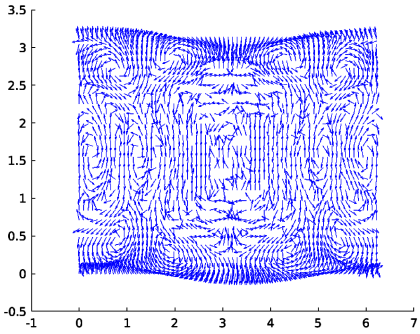

(B) Real Part

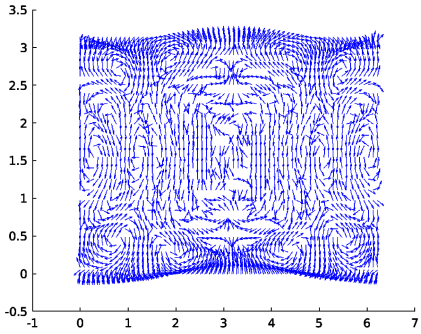

(C) Imaginary Part

FIG. 15. Plot of the calculated complex current's magnitude and quiver plots of its real and imaginary parts

5.3. *Almost non-radiating source.* In the following simulation, we consider the case of an almost radiating source, that is, generating prescribed fields on a near control D_1 while maintaining a near zero field on the far field. Here, D_1 is again the annular sector

$$D_1 = \left\{ (r, \theta, \phi) : r \in [0.012, 0.016], \theta \in \left[\frac{\pi}{4}, \frac{3\pi}{4} \right], \phi \in \left[\frac{3\pi}{4}, \frac{5\pi}{4} \right] \right\}$$

while the far field is $D_2 = \mathbb{R}^3 \setminus B_{10}(\mathbf{0})$, represented by the boundary of the sphere $B_{10}(\mathbf{0})$. The near control D_1 is discretized into 37800 points while D_2 is sampled by a mesh of 3200 elements. In D_1, the prescribed fields are those of the left traveling electromagnetic planewave as described at the beginning of the section. The problem geometry is sketched in Figure 16.

Figure 17 provides a comparison between the prescribed and generated electric fields on D_1. The plots suggest a very good matching in all three components of the electric

fields. Figure 18 verifies this observation as the pointwise relative errors are shown to be in desirable levels, except for some points where the relative errors seem to blow up. It should be noted that those are the points where the fields to be matched are close to zero. The relative L^2 error in the r-, θ-, and ϕ-components are about 3.20×10^{-2}, 1.58×10^{-2}, and 1.20×10^{-2}, respectively.

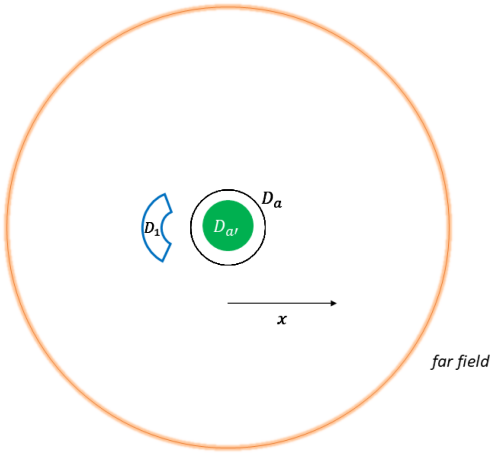

FIG. 16. Sketch of the problem geometry for the case of an almost non-radiating source

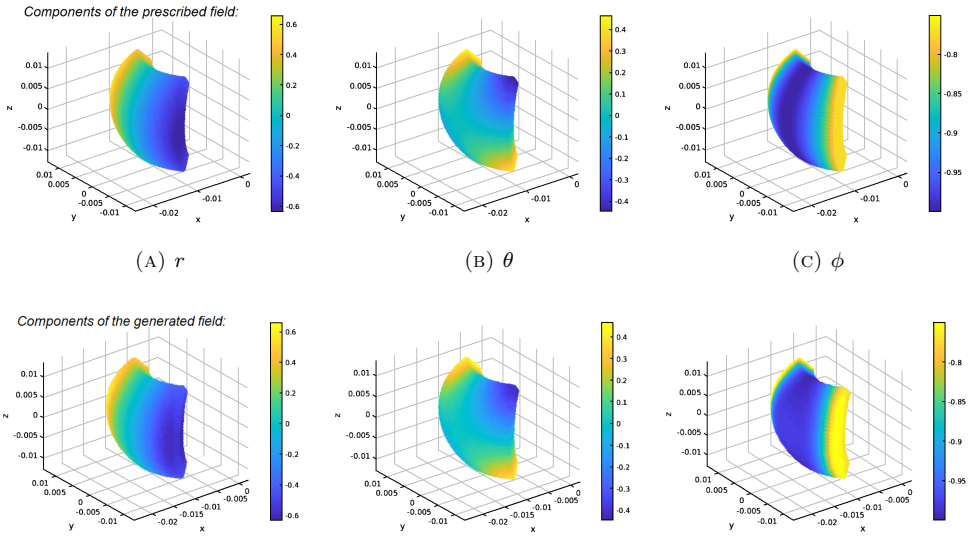

(A) r (B) θ (C) ϕ

(D) r (E) θ (F) ϕ

FIG. 17. Results of the electric field synthesis on D_1

The results for the magnetic field on D_1 are shown in Figures 19 and 20. Figure 19 shows the prescribed and generated magnetic fields. Note that the ϕ-component of the prescribed magnetic field is zero all throughout the near control. The radial component looks to be matched well while there are patches north of the region where the θ-component of the generated magnetic field is a bit off. The ϕ-component is low throughout the region with values of order 10^{-4} and overall L^2 norm of just about 2.15×10^{-5}. The pointwise relative errors for the r- and θ-components are shown in Figure 20. The plots further indicate a good match between the fields. Note that there are points where the r- and θ-components are very small, causing the relative error to appear to be blowing-up. The overall L^2 relative error for the r- and θ-components are nevertheless low with values of 5.96×10^{-2} and 2.70×10^{-2}, respectively.

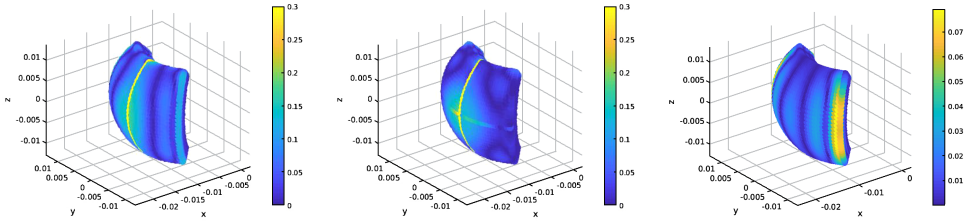

(A) r (B) θ (C) ϕ

FIG. 18. Plots of the pointwise relative errors of the electric field on D_1

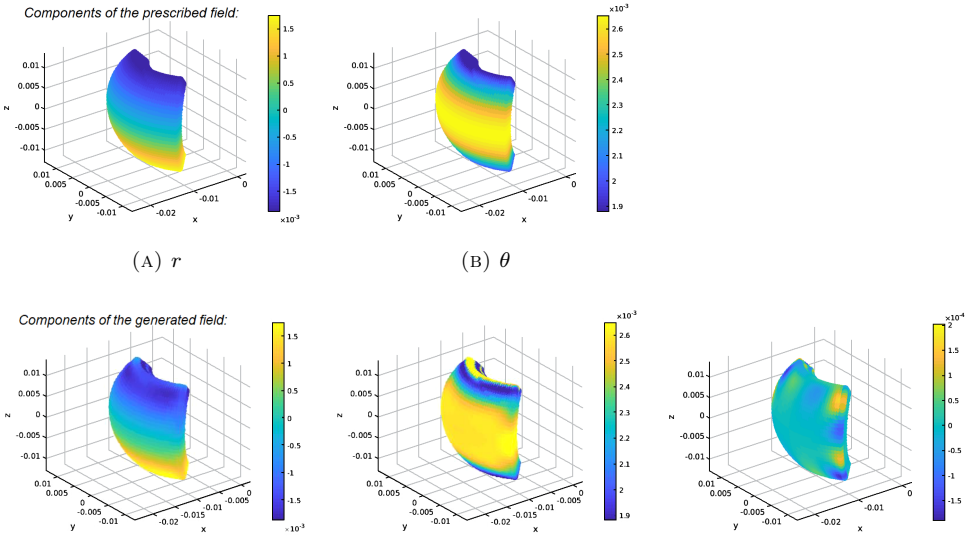

(A) r (B) θ

(C) r (D) θ (E) ϕ

FIG. 19. Results of the magnetic field synthesis on D_1

In the exterior region D_2, we want both the electric and magnetic fields to be very small. Figure 21 shows the three components of the generated electric field on the boundary of D_2, that is, on $\partial B_{10}(\underline{0})$. It can be noted that the field has components of order 10^{-6}. The L^2 norm of the electric field's r-, θ-, and ϕ-components are just about 1.02×10^{-6}, 3.58×10^{-6}, and 9.04×10^{-6}.

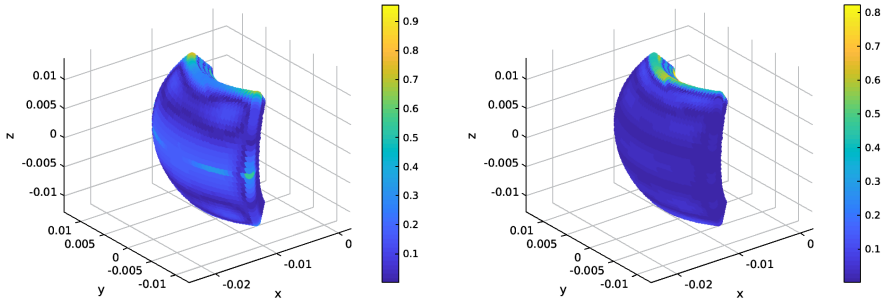

(A) r-component (B) θ-component

FIG. 20. Plots of the pointwise relative errors of the magnetic field on D_1

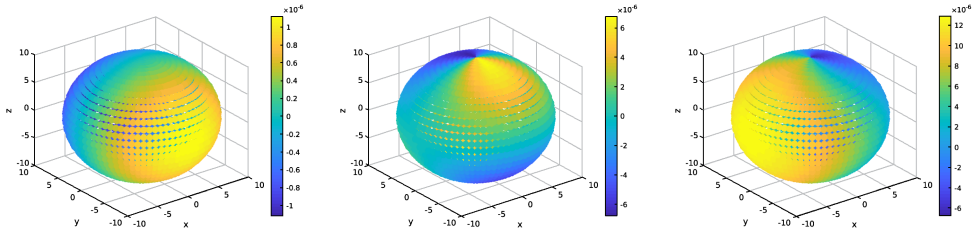

(A) r (B) θ (C) ϕ

FIG. 21. Components of the generated electric field on D_2

In Figure 22, the components of the generated magnetic field are plotted. We can observe values that are even smaller than the components of the electric field. The r-component has values of order 10^{-9} while the θ- and ϕ-components have values of order 10^{-8}. The respective L^2 norm of the r-, θ-, and ϕ-components are 2.47×10^{-9}, 2.40×10^{-8}, and 9.59×10^{-9}.

The next figure describes the complex current needed to generate the results above. Figure 23(A) shows a color map of the magnitude of the complex current in the $\theta\phi$-plane. The magnitude of the current reaches values of over 7×10^4. Figure 23(B) and Figure 23(C) show quiver plots of the magnetic surface currents' real and imaginary parts, respectively.

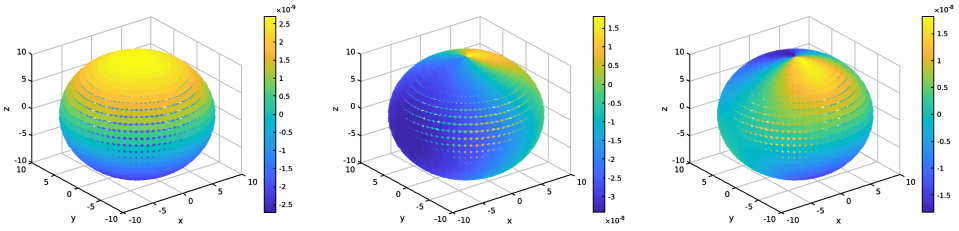

(A) r (B) θ (C) ϕ

FIG. 22. Components of the generated magnetic field on D_2

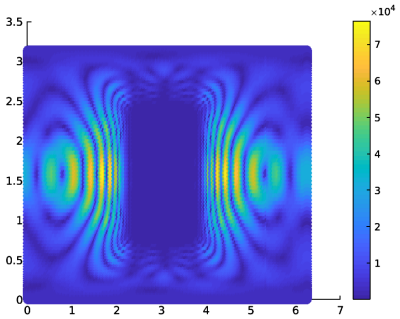

(A) Magnitude

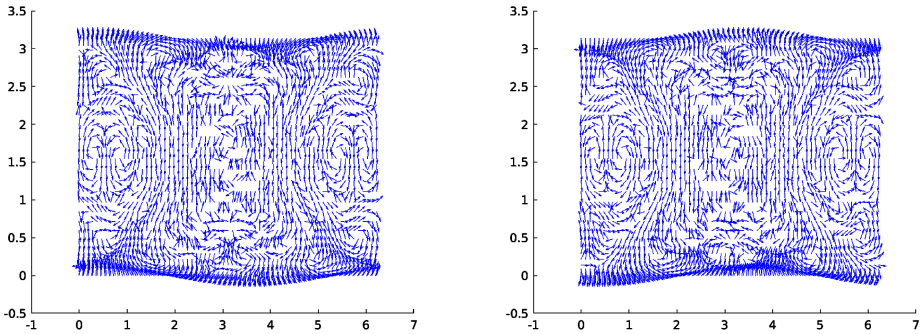

(B) Real part (C) Imaginary part

FIG. 23. Plot of the calculated complex current's magnitude and quiver plots of its real and imaginary parts

6. Conclusion. In this paper, we have established a general way of controlling time harmonic electromagnetic fields in regions exterior to a compact source by determining the necessary surface current on the source. We proposed two possible methods for the computation of the necessary surface currents for the desired control effects: one method

using Debye decomposition of the electromagnetic fields and the second using the integral representation of the electromagnetic fields.

The method we decided to explore numerically requires that the prescribed $(\mathbf{E}, \mathbf{H})$ fields be expressed in terms of Debye (scalar) Helmholtz potentials (u, v), which can be approximated by the methods proposed in [52], [53], and [25]. In turn, u and v were used to calculate the required magnetic (or the conduction) surface current together with the electric and magnetic fields approximating the prescribed fields $(\mathbf{E}, \mathbf{H})$. Thus, the numerical simulations supporting our theoretical results followed the framework discussed in Section 4 in the context of the Morozov discrepancy principle-based Tikhonov regularization used in [52], [53], and [25]. Three geometric configurations were considered in the numerical tests: (1) a single region synthesis where the fields of a prescribed electromagnetic plane wave were approximated in a bounded exterior region, (2) a double region synthesis where the plane wave fields were approximated in a near field bounded exterior region while maintaining low-magnitude fields in another exterior bounded control region, and (3) the case of an almost non-radiating source where fields of an electromagnetic plane wave were approximated in a bounded control region while maintaining very low-magnitude fields in the far field. In all of these configurations, good results were obtained affirming the possibility of controlling EM fields and the feasibility of the proposed numerical schemes.

A possible follow-up to this study is the development of strategies to improve the proposed numerical scheme. For instance, as the frequency increases the numerics generally becomes unstable. This can be mitigated by increasing the harmonic order used in the representation of the unknown density. However, this will greatly increase the computation time. Hence, exploring the use of other basis functions may be warranted. This may also solve the numerical instability caused by the near-singular integrals involved whenever one of the control regions become very close to the source. The authors also intend to perform a detailed sensitivity analysis of the proposed schemes to check its robustness with respect to variations in some of the problem parameters such as the distance between the control regions and the source, the size of the control region, and the frequency. A sensitivity analysis for the scalar case with respect to the aforementioned parameters was performed in [25]. Hence, it will be worthwhile to see if this analysis extends to the vectorial case.

This work can lead to several interesting applications such as in the fields of remote sensing, medical and subsurface imaging, and radar systems. In forthcoming reports, the authors will present related results in the context of sensitivity analysis of the numerical scheme, scattering analysis, and Fourier synthesis towards field manipulation in the time-domain for RCS (radar cross section) reduction and decoy applications, applications to more complex geometric configurations, and the possible use of an array or swarms of moving sources (possibly by employing the second strategy described in Section 3).

References

[1] M. Abramowitz and I. A. Stegun, *Handbook of mathematical functions with formulas, graphs, and mathematical tables*, National Bureau of Standards Applied Mathematics Series, vol. 55, For sale by the Superintendent of Documents, U.S. Government Printing Office, Washington, D.C., 1964. MR0167642

[2] M. Alian and H. Oraizi, *Electromagnetic multiple pec object scattering using equivalence principle and addition theorem for spherical wave harmonics*, IEEE Transactions on Antennas and Propagation **66** (2018), no. 11, 6233–6243.

[3] H. Ammari, H. Kang, H. Lee, M. Lim, and S. Yu, *Enhancement of near cloaking for the full Maxwell equations*, SIAM J. Appl. Math. **73** (2013), no. 6, 2055–2076, DOI 10.1137/120903610. MR3127003

[4] H. Ammari, M. Ruiz, S. Yu, and H. Zhang, *Mathematical analysis of plasmonic resonances for nanoparticles: the full Maxwell equations*, J. Differential Equations **261** (2016), no. 6, 3615–3669, DOI 10.1016/j.jde.2016.05.036. MR3527640

[5] H. Ammari, M. S. Vogelius, and D. Volkov, *Asymptotic formulas for perturbations in the electromagnetic fields due to the presence of inhomogeneities of small diameter. II. The full Maxwell equations*, J. Math. Pures Appl. (9) **80** (2001), no. 8, 769–814, DOI 10.1016/S0021-7824(01)01217-X. MR1860816

[6] H. Ammari, W. Wu, and S. Yu, *Double-negative electromagnetic metamaterials due to chirality*, Quart. Appl. Math. **77** (2019), no. 1, 105–130, DOI 10.1090/qam/1516. MR3897921

[7] T. S. Angell and A. Kirsch, *Optimization methods in electromagnetic radiation*, Springer Monographs in Mathematics, Springer-Verlag, New York, 2004. MR2026856

[8] A. Anikushyn and M. Pokojovy, *Global well-posedness and exponential stability for heterogeneous anisotropic Maxwell's equations under a nonlinear boundary feedback with delay*, J. Math. Anal. Appl. **475** (2019), no. 1, 278–312, DOI 10.1016/j.jmaa.2019.02.042. MR3944321

[9] C. A. Balanis, *Advanced engineering electromagnetics*, Second Edition, Wiley Interscience, 2012.

[10] A. Bensoussan, G. Da Prato, M. C. Delfour, and S. K. Mitter, *Representation and control of infinite dimensional systems*, 2nd ed., Systems & Control: Foundations & Applications, Birkhäuser Boston, Inc., Boston, MA, 2007. MR2273323

[11] W. Cai and V. Shalaev, *Optical metamaterials: Fundamentals and applications*, 1st ed., Springer-Verlag, 2010.

[12] S. Clauzier, S. M. Mikki, and Y. M. M. Antar, *Design of near-field synthesis arrays through global optimization*, IEEE Trans. Antennas and Propagation **63** (2015), no. 1, 151–165, DOI 10.1109/TAP.2014.2367536. MR3301535

[13] D. L. Colton and R. Kress, *Integral equation methods in scattering theory*, Pure and Applied Mathematics (New York), John Wiley & Sons, Inc., New York, 1983. A Wiley-Interscience Publication. MR700400

[14] D. Colton and R. Kress, *Inverse acoustic and electromagnetic scattering theory*, 3rd ed., Applied Mathematical Sciences, vol. 93, Springer, New York, 2013. MR2986407

[15] P. Courilleau and T. Horsin Molinaro, *On the controllability for Maxwell's equations in specific media* (English, with English and French summaries), C. R. Math. Acad. Sci. Paris **341** (2005), no. 11, 665–668, DOI 10.1016/j.crma.2005.10.011. MR2183345

[16] R. V. Craster and S. Guenneau, *Acoustic metamaterials: Negative refraction, imaging, lensing and cloaking*, Springer, 2013.

[17] S. A Cummer and D. Schurig, *One path to acoustic cloaking*, New Journal of Physics **9** (2007), no. 3.

[18] M. Darbas, O. Goubet, and S. Lohrengel, *Exact boundary controllability of the second-order Maxwell system: theory and numerical simulation*, Comput. Math. Appl. **63** (2012), no. 7, 1212–1237, DOI 10.1016/j.camwa.2011.12.046. MR2900096

[19] M. Darbas and S. Lohrengel, *Numerical reconstruction of small perturbations in the electromagnetic coefficients of a dielectric material*, J. Comput. Math. **32** (2014), no. 1, 21–38, DOI 10.4208/jcm.1309-m4378. MR3164915

[20] A. J. Devaney, *Nonradiating surface sources*, J. Opt. Soc. Amer. A **21** (2004), no. 11, 2216–2222, DOI 10.1364/JOSAA.21.002216. MR2122596

[21] A. J. Devaney, *Mathematical foundations of imaging, tomography and wavefield inversion*, Cambridge University Press, Cambridge, 2012. MR2975719

[22] A. Doicu, T. Wriedt, and I. Eremin, *Acoustic and electromagnetic scattering analysis using discrete sources*, Springer Monographs in Mathematics, London: Academic Press, 2000.
[23] L. Dolin, *On the possibility of comparison of three-dimensional electromagnetic systems with nonuniform anisotropic filling*, Izv. Vyssh. Uchebn. Zaved. Radiofiz. **4** (196101), 964–967.
[24] J. Du, S. Liu, and Z. Lin, *Broadband optical cloak and illusion created by the low order active sources*, Opt. Express **20** (2012), no. 8, 8608–8617.
[25] N. J. A. Egarguin, D. Onofrei, and E. Platt, *Sensitivity analysis for the active manipulation of helmholtz fields in 3d*, Inverse Problems in Science and Engineering (2018).
[26] Eng Swee Siah, M. Sasena, J. L. Volakis, P. Y. Papalambros, and R. W. Wiese, *Fast parameter optimization of large-scale electromagnetic objects using direct with kriging metamodeling*, IEEE Transactions on Microwave Theory and Techniques **52** (2004), no. 1, 276–285.
[27] N. Engheta and R. W Ziolkowski, *Metamaterials: Physics and engineering explorations*, Wiley-Interscience, 2006.
[28] A. Epstein and G. V. Eleftheriades, *Huygens' metasurfaces via the equivalence principle: design and applications*, J. Opt. Soc. Am. B **33** (2016), no. 2, A31–A50.
[29] Feng Ling, Chao-Fu Wang, and Jian-Ming Jin, *An efficient algorithm for analyzing large-scale microstrip structures using adaptive integral method combined with discrete complex-image method*, IEEE Transactions on Microwave Theory and Techniques **48** (2000), no. 5, 832–839.
[30] A. Greenleaf, M. Lassas, and G. Uhlmann, *Anisotropic conductivities that cannot be detected by eit.*, Physiological measurement **24 2** (2003), 413–419.
[31] T. B. Hansen and A. D. Yaghjian, *Plane-wave theory of time-domain fields*, IEEE Press Series on Electromagnetic Wave Theory, IEEE Press, New York, 1999. Near-field scanning applications. MR1767418
[32] M. Hubenthal and D. Onofrei, *Sensitivity analysis for active control of the Helmholtz equation*, Appl. Numer. Math. **106** (2016), 1–23, DOI 10.1016/j.apnum.2016.03.003. MR3499954
[33] S. S. Krigman and C. E. Wayne, *Boundary controllability of Maxwell's equations with nonzero conductivity inside a cube. I. Spectral controllability*, J. Math. Anal. Appl. **329** (2007), no. 2, 1375–1396, DOI 10.1016/j.jmaa.2006.06.101. MR2294900
[34] S. S. Krigman and C. E. Wayne, *Boundary controllability of Maxwell's equations with nonzero conductivity inside a cube. II. Lack of exact controllability and controllability for very smooth solutions*, J. Math. Anal. Appl. **329** (2007), no. 2, 1355–1374, DOI 10.1016/j.jmaa.2006.06.102. MR2296930
[35] J. E. Lagnese, *Exact boundary controllability of Maxwell's equations in a general region*, SIAM J. Control Optim. **27** (1989), no. 2, 374–388, DOI 10.1137/0327019. MR984833
[36] I. Lasiecka and R. Triggiani, *Control theory for partial differential equations: continuous and approximation theories. I*, Abstract parabolic systems, Encyclopedia of Mathematics and its Applications, vol. 74, Cambridge University Press, Cambridge, 2000. MR1745475
[37] S. W. Lee, J. Boersma, C. L. Law, and G. A. Deschamps, *Singularity in Green's function and its numerical evaluation*, IEEE Trans. Antennas and Propagation **28** (1980), no. 3, 311–317, DOI 10.1109/TAP.1980.1142342. MR574002
[38] J.-L. Lions, *Contrôle optimal de systèmes gouvernés par des équations aux dérivées partielles* (French), Avant propos de P. Lelong, Dunod, Paris; Gauthier-Villars, Paris, 1968. MR0244606
[39] J. Ma, Z. Nie, and X. Sun, *Efficient modeling of large-scale electromagnetic well-logging problems using an improved nonconformal fem-ddm*, IEEE Transactions on Geoscience and Remote Sensing **52** (2014), no. 3, 1825–1833.
[40] Q. Ma, Z. Mei, S. Kui Zhu, T. Yu Jin, and T. Jun Cui, *Experiments on active cloaking and illusion for laplace equation*, Physical review letters **111** (201310), 173901.
[41] E. A. Marengo and A. J. Devaney, *The inverse source problem of electromagnetics: linear inversion formulation and minimum energy solution*, IEEE Trans. Antennas and Propagation **47** (1999), no. 2, 410–412, DOI 10.1109/8.761085. MR1686310
[42] E. A. Marengo, A. J. Devaney, and F. K. Gruber, *Inverse source problem with reactive power constraint*, IEEE Trans. Antennas and Propagation **52** (2004), no. 6, 1586–1595, DOI 10.1109/TAP.2004.829408. MR2071404

[43] E. A. Marengo and R. W. Ziolkowski, *Nonradiating and minimum energy sources and their fields: generalized source inversion theory and applications*, IEEE Trans. Antennas and Propagation **48** (2000), no. 10, 1553–1562, DOI 10.1109/8.899672. MR1809079

[44] S. M. Mikki and Y. M. M. Antar, *A theory of antenna electromagnetic near field—Part II*, IEEE Trans. Antennas and Propagation **59** (2011), no. 12, 4706–4724, DOI 10.1109/TAP.2011.2165500. MR2907047

[45] R. Mittra and R. K. Gordon, *Radar scattering from bodies of revolution using an efficient partial differential equation algorithm*, IEEE Transactions on Antennas and Propagation **37** (1989), no. 5, 538–545.

[46] R. Mittra and O. Ramahi, *Absorbing boundary conditions for the direct solution of partial differential equations arising in electromagnetic scattering problems*, Progress In Electromagnetics Research **02** (1990), 133–173.

[47] S. N. Mosley, *Alternative potentials for the electromagnetic field*, J. Math. Phys. **39** (1998), no. 5, 2702–2713, DOI 10.1063/1.532415. MR1621454

[48] S. Nicaise, *Exact boundary controllability of Maxwell's equations in heterogeneous media and an application to an inverse source problem*, SIAM J. Control Optim. **38** (2000), no. 4, 1145–1170, DOI 10.1137/S0363012998344373. MR1760064

[49] J. Niitsuma, *Generalized integral formulation of electromagnetic cartesian multipole moments*, Journal of Electromagnetic Waves and Applications (2013), 1–9.

[50] A. N. Norris, F. A. Amirkulova, and W. J. Parnell, *Source amplitudes for active exterior cloaking*, Inverse Problems **28** (2012), no. 10, 105002, 20, DOI 10.1088/0266-5611/28/10/105002. MR2974016

[51] M. O'Neil, *A generalized Debye source approach to electromagnetic scattering in layered media*, J. Math. Phys. **55** (2014), no. 1, 012901, 16, DOI 10.1063/1.4862747. MR3390430

[52] D. Onofrei, *Active manipulation of fields modeled by the Helmholtz equation*, J. Integral Equations Appl. **26** (2014), no. 4, 553–579, DOI 10.1216/JIE-2014-26-4-553. MR3299831

[53] D. Onofrei and E. Platt, *On the synthesis of acoustic sources with controllable near fields*, Wave Motion **77** (2018), 12–27, DOI 10.1016/j.wavemoti.2017.10.004. MR3754438

[54] J. B. Pendry, D. Schurig, and D. R. Smith, *Controlling electromagnetic fields*, Science **312** (2006), no. 5781, 1780–1782, DOI 10.1126/science.1125907. MR2237570

[55] V. Romero-Garcia and A.-C. Hladky-Hennion, *Fundamentals and applications of acoustic metamaterials: From seismic to radio frequency*, Wiley-Interscience, 2019.

[56] E. G. P. Rowe, *Decomposition of vector fields by scalar potentials*, J. Phys. A **12** (1979), no. 1, 145–150. MR518538

[57] S. S. Krigman, *Exact boundary controllability of Maxwell's equations with weak conductivity in the heterogeneous medium inside a general domain*, Discrete Contin. Dyn. Syst. Dynamical systems and differential equations. Proceedings of the 6th AIMS International Conference, suppl. (2007), 590–601. MR2409895

[58] K. Sakoda, *Electromagnetic metamaterials: Modern insights into macroscopic electromagnetic fields*, Springer Series in Materials Science, Springer, 2019.

[59] M. Selvanayagam and G. V. Eleftheriades, *An active electromagnetic cloak using the equivalence principle*, IEEE Antennas and Wireless Propagation Letters **11** (2012), 1226–1229.

[60] M. Selvanayagam and G. V. Eleftheriades, *Experimental demonstration of active electromagnetic cloaking*, Phys. Rev. X **3** (2013), 041011.

[61] V. P. Smyshlyaev, *The high-frequency diffraction of electromagnetic waves by cones of arbitrary cross sections*, SIAM J. Appl. Math. **53** (1993), no. 3, 670–688, DOI 10.1137/0153034. MR1218379

[62] T. Su, L. Du, and R. Chen, *Electromagnetic scattering for multiple PEC bodies of revolution using equivalence principle algorithm*, IEEE Trans. Antennas and Propagation **62** (2014), no. 5, 2736–2744, DOI 10.1109/TAP.2014.2308522. MR3209123

[63] T. Su, J. Wang, J. Chen, R. Chen, and W. Wang, *Fast computation of em scattering from an uav swarm*, 2019 IEEE international conference on computational electromagnetics (ICCEM), 2019, pp. 1–3.

[64] W. Wei, H.-M. Yin, and J. Tang, *An optimal control problem for microwave heating*, Nonlinear Anal. **75** (2012), no. 4, 2024–2036, DOI 10.1016/j.na.2011.10.003. MR2870896

[65] C. H. Wilcox, *Debye potentials*, J. Math. Mech. **6** (1957), 167–201, DOI 10.1512/iumj.1957.6.56007. MR0087462

[66] Y. Xu, H. Yang, R. Shen, L. Zhu, and X. Huang, *Scattering analysis of multiobject electromagnetic systems using stepwise method of moment*, IEEE Transactions on Antennas and Propagation **67** (2019), no. 3, 1740–1747.

[67] A. D. Yaghjian, *Electric dyadic green's functions in the source region*, Proceedings of the IEEE **68** (1980), no. 2, 248–263.

[68] R. Zhao, Z. X. Huang, Y. P. Chen, and J. Hu, *Solving electromagnetic scattering from complex composite objects with domain decomposition method based on hybrid surface integral equations*, Eng. Anal. Bound. Elem. **85** (2017), 99–104, DOI 10.1016/j.enganabound.2017.09.014. MR3719416